SLAC-PUB-1432
(E/A)
May 1974

MUON SHIELDING AROUND HIGH ENERGY ELECTRON ACCELERATORS: PART II: EXPERIMENTAL INVESTIGATION*

W. R. Nelson**, K. R. Kase†, and G. K. Svensson††

Stanford Linear Accelerator Center
Stanford University, Stanford, California 94305

ABSTRACT

This paper describes and presents results of an experiment measuring the fluence and absorbed dose delivered by electron accelerator-produced muons penetrating thick iron shields. The experiment was designed to check the theoretical calculations described in the preceding paper. Nuclear track emulsions and scintillation counters were used to measure fluence and ^{7}LiF was used for the dose measurement. It is shown that the absorbed dose can be calculated from the fluence data by using a restricted stopping power. The results of the measurements indicate that the theoretical calculation accurately predicts the muon fluence and absorbed dose at small angles (<30 milliradians) but underestimates both at large angles by an order of magnitude or more. Several possible explanations for this effect are discussed.

(Submitted to Nucl. Instr. and Meth.)

* Work supported by the U. S. Atomic Energy Commission.
** Submitted as partial fulfillment of the degree of Doctor of Philosophy at Stanford University.
† Present Address: Stanford University Medical Center, Stanford University, Stanford, California 94305.
†† Present Address: Joint Center for Radiation Therapy, Department of Radiation Therapy, Harvard Medical School, 50 Binney Street, Boston, Massachusetts 02115.

1. Introduction

In this paper we present the results of an experiment designed to accurately measure the fluence of and the absorbed dose from electron accelerator-produced muons that penetrate massive iron shields. A theoretical formulation of the problem has been presented in the paper preceding this one, which shall be referred to as Paper I. The investigation presented here shall be referred to as Paper II, and is similar to an experiment published in 1968 by one of the authors (Nelson 1968). With regards to the 1968 study, it was found that the Nelson theory, as well as a more general theory of Alsmiller (1969), disagreed quite distinctly with the data presented. Since the Nelson and Alsmiller models were essentially the same, it was considered necessary to repeat the experiment in a more precise and controlled way.

The present experiment uses nuclear track emulsions and scintillation counters to measure the muon fluence, and thermoluminescent dosimeters to measure the absorbed dose. Measurements lateral to the incident beam direction are made at four iron shield thicknesses ranging from 5 to 7 meters. The results are compared with the theory presented in Paper I.

2. General Description of the Experiment

2.1 Overall Layout and Dump-Target Arrangement

The general layout of the experiment is given in Figure 1, which shows a plan view of the shielding that separates the inside of End Station B (ESB) on the right from the B Target Room (BTR) on the left. The electron beam traversed the BTR from left to right and was absorbed in beam dump 8T2, which was the source of muons for this experiment. Figures 2 and 3 are section views of Figure 1.

The dump consisted of 38 copper discs, ranging in thickness from 0.64 to 3.81 cm, that were spaced inside a 15.24 cm diameter closed stainless steel cylinder in such a manner as to allow ample water flow for heat transfer purposes. This cylinder was surrounded radially by lead shielding and was enclosed in another stainless steel cylinder such that the overall length of the dump was 91.94 cm and the diameter was 36.83 cm. The muons were assumed to be produced at a point located 22.23 cm from the upstream face of the dump, corresponding to a target thickness of 6 radiation lengths (according to the data given by Tsai and Whitis (1966), at least 95% of the muons that are capable of penetrating the iron shield will have been produced within 6 radiation lengths). The remaining material downstream of this point source totaled 61.70 cm (Fe-equivalent by density), which was considered to be part of the iron wall thickness. Table 1 gives the total iron thicknesses and the source-to-detector distances. The radiation length values used were calculated by Dovzhenko and Pomanskii (1964).

2.2 Charge and Beam Position Monitoring

The electron beam was monitored with SLAC charge monitor 8I1. The charge monitoring circuit is similar to that described in detail by Larsen and Horelick (1968). Passage of a beam pulse through the toroid induces a signal which is proportional to the beam current, and this output is integrated on a pulse-to-pulse basis to a nominal ±1% over a 35-dB range. Faraday cup comparisons have been made at SLAC (Larsen and Horelick 1968) for currents greater than 1 mA peak, and they show agreement to less than 1%.

Monitoring the position and direction of the beam was accomplished by establishing the beam at the center of several microwave position monitors (Larsen 1966) and visual position monitors (e.g., ZnS screens and Cerenkov

monitors), which are situated along the beam line at key locations, including the upstream face of the dump-target 8T2. The center of the ZnS screen on 8T2 was accurately positioned on a theoretical line passing through the center of upstream position monitors (this line had been used on other experiments for several years with success). Furthermore, the detector positions downstream of the shielding were also defined on this line prior to the stacking of the iron shielding wall. During the early phase of the experiment, before the integrating detectors were exposed, the beam steering and alignment was checked using two scintillation counters located downstream of the shielding.

2.3 Energy Resolution

The beam pulses from the accelerator structure are channeled into the various experimental areas by means of a magnetic transport system (Harris et al. 1968). The energy of the B-beam is defined by the transport system (magnets plus collimators) to a nominal accuracy of $\pm 0.5\%$. To avoid the possibility of producing an additional source of muons at the final energy slit, located far upstream of the dump-target (8T2), the slit was opened to its widest position in energy resolution (namely, $\pm 2.5\%$ (HWHM)). The initial beam was established at $\pm 0.5\%$; however, there is no guarantee that it stayed that way throughout the exposures. The beam spot that was observed on the dump ZnS screen (8PR2) by means of closed-circuit TV was carefully watched and found to be extremely stable during each exposure. Therefore, we believe that the 18 and 14 GeV beam energies used in this experiment were known to at least $\pm 1\%$ (HWHM).

2.4 Detector and Shielding Arrangement

Since the main purpose of this experiment is to measure the lateral distribution of the fluence of muons that penetrate massive iron shielding, it was

important to locate the detectors in a precise way, especially in the direction perpendicular to the incident electron beam axis. To accomplish this the following arrangement was used. First, detector stands were constructed out of kiln-dried wood as shown in Figure 4 (mounted in place in End Station B prior to the stacking of the steel blocks). The portion of the frame nearest the target (see Figure 2) was designated as Stand A (corresponding to Gap A) and the others B, C, and D, respectively (note: Gap D was not really a gap). Since calculations indicated that the fluence would vary by about four orders of magnitude throughout the shielding array, a series of exposures was planned. This entailed removing groups of detectors during the course of the experiment. To accomplish this in a convenient, but still precise, way the detectors (nuclear track emulsions and thermoluminescent dosimeters) were mounted inside wooden blocks. The blocks, in turn, were accurately positioned on each stand by means of wooden pegs as shown in Figure 4.

The fluence was measured at an angle 10 degrees to the vertical in all four gaps, as well as horizontally in Gaps A and D. The horizontal measurement provided a means of checking the symmetry of the muon fluence. This was particularly important to do since any additional source of muons (such as the energy slit described above) would be more apparent in the horizontal plane because the electron beam was steered horizontally into dump 8T2. This is easily seen in Figure 1 where the nominal forward direction of the primary electron beam is designated as BEAM LINE 2.

Three blocks, designated I, II, and III, were positioned along each arm of the frame — block I was the block closest to the beam centerline. As an example of the numbering system, block A-II-H was the block located in position II of the horizontal stand in Gap A.

The stand-array system was aligned by the SLAC precision alignment crew to ± 0.13 cm, relative to the primary beam direction. The blocks in position I along each vertical arm extended through the beam axis, thus allowing for later measurement to indicate a misalignment. A three dimensional stack of nuclear track emulsion, as well as an emulsion plate whose plane was perpendicular to the beam direction, were exposed to what was assumed to be the beam centerline. Subsequent discovery of a misalignment of the detectors relative to the beam could, therefore, be corrected for in the data analysis. This was not found to be necessary, however.

In addition to the detector stands for the emulsions and TLD's, two scintillation counters (labeled SC1 and SC2) were positioned in Gap A a distance of 7.6 cm in front of the emulsion-TLD stand and along the horizontal direction. SC1 was aligned with the beam centerline and SC2 was located at the extreme end of the lateral measurement (a displacement of 83.82 cm from the beam axis). Since we had to allow for removal of the counters should electronic difficulties arise, a special stand was constructed for them. This stand made it quite easy to quickly and accurately re-align the counters — even though they had to be lowered to a depth of 2 meters inside an 18 cm gap. Furthermore, this made it possible to interchange the counters with one another as a check on their relative response to the same radiation field.

Finally, the detector stand-array was bolted in place during the alignment phase and iron blocks (approximately 74 cm thick) were stacked around the wooden frame. The alignment was checked and maintained during the course of the stacking of the iron (note: after the experiment was over and the iron had been carefully removed, the alignment was re-checked and was found to be the same). Figure 5 shows the iron in place with the detector stand-array protruding from the gaps.

2.5 Main Shielding Wall (Beam Port Funnel) and Background Shielding

The main shielding wall that separates End Station B from the dump-target (8T2), located in the B Target Room, is shown in Figure 1. This plan view shows that the iron wall extends well past 150 milliradians in horizontal angle, which is the widest location of detectors in this experiment. In fact, the iron horizontally fills the entire space labeled BEAM PORT FUNNEL. Section A-A (Figure 2) gives the elevation view and shows that the iron portion of the port funnel shielding extends only 91 cm above and 30 cm below the beam centerline. A vertical angle of 150 milliradians is shown in Section A-A and it is clear that there is enough steel to completely cover any direct ray from the source to the detectors within a polar angle of 150 milliradians.

A void in the iron portion of the port funnel shielding, approximately 22 cm by 61 cm by 213 cm, is shown in Figures 1 and 2. It was discovered when the beam port funnel was being reconstructed for another experiment — several months after the exposures had been made. The effect of this void on the experimental results will be discussed later.

To eliminate as much background radiation as possible, the beam port funnel was re-built from its normal three-port configuration to a solid wall with only a single port, as shown. This beam port (BEAM LINE 2 in Figure 1) was needed for an experiment that was on the SLAC schedule following ours. To attenuate the radiation that might stream down this hole, tightly fitting lead plugs were installed at both ends (approximately 90 cm total) as depicted in Figure 1.

As a further protection against background radiation, Gaps A through C were covered on the sides and on the top with lead blocks (at least 20 cm on the sides and 10 cm on top). Gap D was left exposed.

2.6 Detectors — Scintillation Counters

Two identical scintillation counters (SC1 and SC2) were built to measure the muon fluence prior to and during the emulsion/TLD exposures. In addition to providing an independent means of measuring the fluence, the scintillation counters made it much easier to determine the correct exposures. Both counters were constructed of Pilot B plastic (1 cm^2 × 0.64 cm) that was optically coupled to the face of a RCA-8575 photomultiplier tube. Ortec Model 270 tube bases were used. The total error in alignment is estimated to be less than ± 0.16 cm. A block diagram of the electronic components used in conjunction with the counters, as well as data relating to counter plateaus and efficiencies, has been described in detail elsewhere (Nelson 1973).

2.7 Detectors — Nuclear Track Emulsion

Nuclear track emulsion has been routinely used to measure the fluence of charged particles and neutrons around high energy accelerators. In the present study, Ilford G.5 emulsion plates (400 microns thick) were positioned throughout the gaps in the iron shielding stack described above. After exposure and development, the muon tracks were counted using a microscope and the muon fluence distribution was obtained. Figure 6 is a photomicrograph showing two muon tracks in the center and one at the left edge. Details, such as alignment of the emulsion, microscope optics, emulsion development, track counting techniques, absolute and relative scanning efficiencies, and the weighting and combining of data from various scanners has been adequately described elsewhere (Nelson 1973).

2.8 Detectors — Thermoluminescent Dosimeters

Approximately 120-130 mg of TLD-700 phosphor (Harshaw Chemical Co., Cleveland, Ohio) was loaded into polyethylene capsules (0.51 cm (O.D.) × 0.30 cm (I.D.) × 2.29 cm long). These capsules were positioned within holes that were

bored in the wooden blocks that held the emulsion plates. The holes were bored on the downstream side of each wooden block in a direction such that the capsule length was approximately oriented along the incident beam direction. Several duplicate blocks, containing TLD capsules but without nuclear emulsion, were made-up so that longer exposures could be attempted. The phosphor had been pre-annealed for one hour at 350 degrees C and for 24 hours at 80-90 degrees C (Svensson et al. 1970).

Several capsules were stored along with the main TLD capsules to determine the radiation dose not attributed to the muon exposures. A total of ten readings were taken along with dark current and light source measurements. The average background dose on the TLD's was determined to be 71.1 ($\pm$5.0) mrad, which was subtracted from the muon-exposed TLD dose measurements.

The TLD capsules were read-out over a period of about one week immediately after the background dose above was determined. Four separate readings on each capsule were averaged (in most cases). The planchet and TLD reader were allowed to cool between read-outs, and the dispenser was cleaned out with pressurized dry nitrogen gas between capsules. A dark current reading was taken at intervals and subtracted from the average reading for each capsule.

The TLD's were calibrated by determining their sensitivity for an absorbed dose of one rad from a ^{60}Co source (Nelson 1973). It had been predetermined, using the muon fluence data obtained from the scintillation counters and the nuclear track emulsions, that the highest absorbed dose reading on the TLD's would not exceed 25 rad. Therefore, it was not necessary to correct for increased sensitivity at high doses (supralinearity).

3. Results and Comparison With Theory

3.1 Muon Fluence Measurements

The muon fluence measured in Gap A is shown in Figure 7 as a function of the production angle (refer to Figures 1 through 3 for the geometry). The data have been normalized to the total integrated electron charge that impinged on the beam dump 8T2. The error analysis for the emulsion data has been described elsewhere (Nelson 1973). Three scintillation counter points are also shown. Counters SC1 and SC2 are plotted at 0 and 154 milliradians, respectively. The counter point at 51.8 ($\pm$ 0.5) milliradians was taken several months prior to the main exposures. At that time the iron wall downstream of the beam port funnel shielding had not yet been constructed and a counter was simply positioned in the open, unshielded laterally. The error bar in the θ-direction reflects the uncertainty in its position. All other θ-positions, both counter and emulsion, are known to a much higher accuracy ($\pm$ 0.3 and $\pm$ 0.1 milliradians, respectively).

The solid line in Figure 7 is based on the theoretical formulation developed in Paper I. Only the coherent production of muons is shown since it is the dominant contribution for angles smaller than 120 milliradians, as we shall see in Section 3.5e. Equations (28) through (34) of Paper I form the basis of a computer program called GREEN, which essentially folds-together the production distribution (in energy-angle) and the Fermi-Eyges multiple scattering probability. As we have stated in Paper I, the small angle formulation, published by one of the authors (Nelson 1968) several months prior to that of Alsmiller et al. (1968), was not used as the theoretical basis in this paper. Because of the elegance in Alsmiller's presentation (Alsmiller et al 1968, Alsmiller 1969), and because it does not contain the small angle approximations, we have decided to use it. It should be emphasized, however, that the "model" is the same for both

formulations — namely, the shield multiple scatters the energy-angle distribution according to the Fermi-Eyges theory. For small angles, which we have in this experiment (note: $\theta < 9$ degrees), the two formulations should be quite close. What is new in the theory presented in Paper I is the choice of production cross section. The theory of Kim and Tsai (1972a, 1973) is considerably more accurate than the one previously used by Nelson and by Alsmiller et al.

Keeping in mind that the comparison in Figure 7 between theory and measurement is on an absolute basis, it seems reasonable to say that the theory predicts the muon fluence at small angles, but underestimates the muon fluence as theta increases. At 150 milliradians the theory, in fact, is a factor of 20 to 30 too low. This is also found to be the case in Gaps B, C, and D, as shown in Figures 8 through 10, respectively.

3.2 Absorbed Dose Measurements

The thermoluminescent dosimeter measurements are plotted as a function of the production angle in Figures 11 through 14 and are compared with the theory (coherent production only) presented in Paper I. Except for the points at angles greater than 95 milliradians, the error bars in either direction are smaller than the data points themselves. The points at larger angles have large vertical error bars because the exposure in this region was quite short and the dose was comparable to the background powder dose. (Note: Gaps A and B had short exposures, but C and D were much longer — so the error bars for A and B are quite small everywhere.)

Two theoretical curves are shown in Figures 11 through 14 corresponding to the use of a restricted stopping power (LET_{Δ}) or an unrestricted stopping power (LET_{∞}). We chose Δ to be the energy of an electron whose range in LiF is 1.5 mm — the radial size of a TLD capsule used in this experiment. From

Berger and Seltzer (1964, 1966) we find that $\Delta = 0.8$ MeV. The overall effect of using a restricted stopping power rather than an unrestricted stopping power is a 25% decrease in the theoretical estimate of the absorbed dose at small angles, and about 10% at large angles. The agreement between theory (LET_{Δ}) and experiment at zero milliradians is reasonably good, but the difference at large angles is even more apparent than in the fluence case. Most likely the TLD's have measured a constant "background" radiation component that dominates over the muon dose at large angles. The effect in Gap D is quite pronounced (Figure 14) since, unlike Gaps A, B, and C, there was no lateral shielding.

Presumably the "background" dose comes from photons that scatter over the top of the BTR wall where the shielding was relatively thin (the roof of the BTR consisted of 122 cm of steel with some cracks as large as 1.5 cm). The direct effect of neutrons can be excluded since the TLD (^{7}LiF) responds almost exclusively to charged particle or photon radiation. The neutron fluence would have to have been quite large to produce an indirect effect on the TLD, such as knock-on protons from the wood or capture gamma rays from the iron. Fission track detectors, placed at various locations in the gaps and inside ESB, indicated that the neutron fluence was below the minimum detectable level (6×10^{5} neutrons/cm^{2}) (Gay and Svensson 1970).

It has been stated in Paper I that the fluence-to-absorbed dose factor can be approximated by a constant, and therefore can be taken outside the energy integration (see equation (26) of Paper I). Let us assume this to be the case, and let us compare the fluence data directly with the absorbed dose measurements by normalizing the two at zero milliradians. This is done in Figure 15 where the scintillation counter data and some of the emulsion points from Figure 7

have been plotted on the absorbed does figure for Gap A. This illustrates quite nicely the effect of the background component at large angles. The thermoluminescent dosimeters simply cannot distinguish between muons and low energy photons; whereas, the nuclear track emulsions clearly distinguish muon tracks from low-energy electrons produced by the photons — and the counters apparently do also. A similar background effect was observed in the experiment by Nelson (1968), as discussed in Section 5 of Paper I.

The normalization of the fluence data to the emulsion data in Figure 15 was done using a conversion factor of 2.33×10^{-8} rad-cm^2, corresponding to a restricted stopping power of 1.45 MeV-cm^2/g. This results in a flux density-to-absorbed dose rate factor of 12 muons/cm^2/sec = 1 mrad/hour. This ratio of theoretical dose to theoretical fluence is found to be constant within 4% over the angular range and for the iron thicknesses considered in this experiment so that it is sufficient in practice to calculate the muon fluence and to multiply by a conversion factor to get absorbed dose. The correct factor to use, however, depends on the detector-geometry under consideration, as well as the energy distribution of the muons.

3.3 Muons Photoproduced From Other Targets

The large number of particles at the wide angles could, of course, be due to sources other than the one at dump-target 8T2. Great care was taken to avoid this possibility. However, since it was anticipated when we designed the experiment, the fluence and absorbed dose were measured in two directions. Since the vertical data were measured in a direction almost 90 degrees to the horizontal plane of bend, a direct comparison of the horizontal and vertical data should indicate whether another source is present or not. Because we have symmetric results in both the fluence and absorbed dose measurements, we

rule out additional photo-muon sources as an explanation for the discrepancy between theory and measurement. Later on we will present angular distribution data that will support this conclusion.

3.4 Muons From Pion (Kaon) Decay

Because pions and kaons are photoproduced much more abundantly at large angles than muons are, one must consider the decay of these particles into muons as a possible explanation for the discrepancy between theory and experiment. According to the SLAC Users Handbook (1971), the yield of pions varies with material according to $A^{-0.8}$, so that one would expect about five times as many pions from a beryllium target as from a copper one. On the other hand, one can show from the equations in Paper I that the yield of muons by pair production decreases, but only slightly (15%) in going from a copper target to a beryllium one. Similar arguments hold for the K-yield at large angles. This suggests that a critical test as to the source of muons at large angles would be to put a beryllium target into the beam just in front of the dump-target 8T2 and to observe the effect.

To check this we measured the muon fluence at zero and 154 milliradians with and without one radiation length (35.7 cm) of beryllium in the beam. The measurements were made at incident electron energies of 18 and 14 GeV and the results are given in Table 2 for the two scintillation counters SC1 and SC2. The data show that muons from pion or kaon decay appear predominantly at large angles and support the idea that the muon fluence at wide angles is caused, in part at least, by this source.

Since the beryllium target greatly affects the muon count rate at large angles, it would be reasonable to expect that the muon tracks in the nuclear emulsion should point back towards the source (8T2). Photo-muons that get to

the large angles essentially by scattering in the shield would, on the contrary, point into the shield itself. To verify this idea, angular distribution measurements were made at zero and 7.7 degrees (133.4 milliradians) and the results are shown in Figures 16 and 17, respectively. The histogram in Figure 16 clearly demonstrates that the theoretically established zero degree direction is correct and that the muon angular distribution is symmetric as expected. The histogram in Figure 17 suggests that there are two peaks and possibly an isotropic background. The large peak is located approximately eight degrees relative to the zero degree reference and is consistent with the known source-to-detector angle of 7.7 degrees. The smaller peak occurs at about 22 degrees and presumably is due to photo-muons that have multiple scattered in the shield. Also shown in Figure 17 is a theoretical estimate representing the sum of the background component and the photo-muon component (dashed line). The background component was estimated by track counting the background emulsion and assuming that the tracks are uniformly distributed in angle. The photo-muon contribution was obtained by numerically integrating the Fermi-Eyges distribution (see Equation (14) of Nelson (1968)) over the muon energy spectrum incident upon the shield ($\phi = 0$ degrees), with z and y chosen to be the shield thickness and lateral detector position, respectively, and the lower limit of integration dictated by the shield thickness. This gave an "effective" angular distribution whose area was then normalized according to the ratio of measured-to-theoretical fluence given by Figure 7 at 7.7 degrees.

As we have stated, the dashed line in Figure 17 represents the sum of the scattered photo-muons and the background tracks. It is not surprising that the location of the calculated peak (21.6 degrees) agrees with the second peak in the histogram and that both extreme sides of the measured distribution can be

predicted by the background track distribution. The peak height of the dashed curve, however, is not large enough to account for the second peak in the histogram, suggesting that the area normalization is wrong. At the present time this is not understood. What is clear from these data is that the majority of the muons that reach the detectors located at large angles get there because they emanate from the source at large angles. Several possibilities might explain this. For example, the pair production cross section might be larger at wide production angles than that calculated in the model described in Paper I. Another possibility is that the muons scatter to large angles near the source, either by Coulomb or nuclear interactions. Both of these ideas will be looked at in more detail in later sections.

The possibility that these muon tracks come from the decay of pions (kaons), is certainly suggested by the beryllium target experiment and the angular distribution data. A theoretical calculation of the fluence of muons due to pion (kaon) decay has been presented elsewhere (Nelson 1973), and a comparison with the experimental results of Gap A, as well as with the coherent photo-muon theory, is made in Figure 18. The actual dump-shield geometry was used in the calculation, thereby accounting for decay versus interaction of these hadrons in the water/air gaps. The results are tabulated in Table 3. Unfortunately, the calculations show that neither pion nor kaon decay, nor both together, will account for the additional muons measured at wide angles. It would take at least 30 times the sum of the π/K fluence of muons, at 100 milliradians, to account for the number of muons measured in excess of the coherent pair production theory.

The total number of muons (per Coulomb) can be obtained by integration; namely,

$$N/Q = Q^{-1} \int_{\Delta A} (dn/dA)dA,$$

$$= 2\pi R^2 Q^{-1} \int_0^{\pi} \Phi(\theta) \sin\theta d\theta \qquad (1)$$

where Φ/Q is any one of the four curves in Figure 18. Graphical integration gives the following for Gap A

$$N/Q)_{exp} = 2.17 \times 10^{13} \text{ muons/Coulomb},$$

$$N/Q)_{coh} = 1.64 \times 10^{13} \text{ muons/Coulomb},$$

$$N/Q)_{\pi\mu} = 6.87 \times 10^{10} \text{ muons/Coulomb},$$

and

$$N/Q)_{K\mu} = 1.66 \times 10^{10} \text{ muons/Coulomb}.$$

Obviously the ratio of the experiment to the coherent pair production theory, which is 1.32, cannot be accounted for by either pion or kaon decay muons, or their sum.

3.5 Other Possible Explanations for the Theory/Measurement Discrepancy

In this section, we will consider other possible explanations for the rather large fluence and absorbed dose measurements that have been observed at wide angles.

(a) The Angular Spread of Photons in the Shower

In obtaining the calculated results presented in Paper I, it has been assumed that the angular distribution of the photons in the target can be neglected. The reasons are as follows. The characteristic angle of bremsstrahlung is of the

order

$$\theta_{\gamma} = m/E \approx 0.07 \text{ milliradians},$$

where the electron energy E is determined from the energy of a muon that just gets through the shield at Gap A (i.e., 7 GeV).

Furthermore, the mean angle for multiple scattering in one radiation length is

$$\theta_{ms} \approx 15 \times 10^{-3}/E \text{ (GeV)} \approx 2 \text{ milliradians}.$$

Since these angles are small, relative to the angles at which the discrepancy between experiment and theory occur, shower divergence seems an unlikely answer.

At the suggestion of Nelson (1968), a calculation was made by Alsmiller and Barish (1969) to substantiate this claim. They calculated the angular distribution of the photons in the target using the Monte Carlo shower code written by Zerby and Moran (1962a, 1962b, 1963). They then used this distribution, along with the older version of the photo-muon cross section (Tsai 1971) and the Eyges (1948) multiple scattering formulation, to calculate the muon fluence through a steel shield. The difference between this result and the same calculation, excluding the photon angular distribution, was very small indeed. We can conclude, therefore, that shower divergence does not explain the difference between the theory and the experimental observations presented in this paper.

(b) Hadron and Electron Tracks in the Emulsion

A detailed analysis of the possibility of mistaking hadron and/or electron tracks as muon tracks in the nuclear emulsion has been presented elsewhere (Nelson 1973). It is demonstrated that the over-abundance of tracks at large angles cannot be due to electron or hadron contamination.

(c) The Effect of the Void in the Beam Port Funnel Shielding on the Measurements

As we have pointed out earlier, a void in the main iron shielding wall was discovered several months after the exposures had been made. The void is shown in Figures 1 and 2.

The mathematical formulation that has been developed in Paper I, and the associated computer programming is unable to cope with inhomogeneities in the shield. The formalism developed by Alsmiller et al. (1971) apparently can treat situations of this type. Two effects are involved here. The first is simply a reduction in the shield thickness in the region subtended by the void. The second, and more difficult effect from our calculational point of view, is the unscattered propagation of muons through the void (a moment-arm effect).

We are able to estimate the effect of a decrease in the shielding by simply re-running the computer code with a new shield thickness (see Table 1). We find very little difference ($< 5\%$) when we do this.

The moment-arm effect has not been calculated, but we feel that it is not significant since the void was small in the direction of the beam. To back this up, we see from the measurements made in the vertical and horizontal directions that the muon fluence and absorbed dose is symmetric about the beam direction. Therefore, the void in the shielding cannot be the reason for the discrepancy we have observed.

(d) Single Scattering in the Shield

Multiple scattering can be described as the diffusion process whereby a large number of small-angle Coulomb interactions result in a net deflection on the downstream side of the shield being traversed. Single scattering, on the other hand, is the net result of a large-angle scatter, superimposed upon which

is a large number of relatively insignificant small-angle scatterings. The small-angle multiple scattering theory of Fermi-Eyges (Rossi 1952, Eyges 1948) was used as a basis for the transport theory in Paper I.

In order to evaluate the effectiveness of the Fermi-Eyges theory in describing the transport of muons through the shield, Alsmiller (1969) has performed Monte Carlo calculations using the more fundamental scattering theory of Moliere (1947, 1948). At large angles the Moliere theory approaches the Rutherford Law for scattering from a point charge, and therefore Alsmiller's Monte Carlo approach should bring out the single scattering effects, if they are important. His calculation uses the photo-muon cross section of Tsai (1971) and the geometry used in the first muon experiment performed by Nelson (1968). It is reported by Alsmiller that the Fermi-Eyges theory agrees quite well with the Monte Carlo results, suggesting that single (or plural) scattering effects are not too significant. Several things are worth mentioning, however. First, the calculations published by Alsmiller are only plotted out to a lateral position of 45 centimeters (for a source-to-detector distance of 510 centimeters), corresponding to a detector angle of 88 milliradians. The detector angles in the present experiment, however, go out as far as 154 milliradians. It would be useful if the calculation could be repeated for the situation described by this experiment.

Second, the effect of inelastic scattering in the shield has apparently not been included in the Monte Carlo calculation, and it probably should. Third, the finite size of the nucleus was not considered by Moliere in his theory.

(e) Exact Versus Approximate Theories

As we have indicated in Paper I, the photoproduction of muon pairs is the result of a number of contributions depending on the initial and final state of the

object(s) that accept the momentum transfer in the interaction. In the energy realm being considered in the present experimental study, the main contribution is from an elastic interaction with the nucleus as a whole (coherent contribution). This is the contribution that has been plotted in the figures above. As shown in Paper I, the next important component comes from momentum transfer to a proton (incoherent proton contribution), whereby the process is taken to be elastic. The result is a 40% increase in the fluence at 150 milliradians, which is not nearly enough to obtain agreement with experiment (a factor of 20 to 30 is needed). At 120 milliradians, the elastic proton contribution amounts to less than 10% of the coherent production, and as the angle gets smaller the coherent term completely dominates.

The contribution from the elastic neutron interaction and from the inelastic nucleon interactions are shown to be even smaller in Paper I. Furthermore, using the exact (Born) cross section instead of the Weizsacker-Williams cross section will apparently not help either. As indicated in Paper I, a total increase of 100% over the coherent contribution is the largest expected at 150 milliradians. The approximations that have been made in the theory, therefore, are not the cause of the discrepancy between theory and measurement. This does not rule out the possibility that the cross section itself is incorrect, however.

4. Conclusions

In the preceding sections we have presented the results of an experiment, designed to check the theory given in Paper I, and we have observed the following.

(a) The muon fluence and the absorbed dose in the zero degree direction are correctly predicted by the theoretical model for an iron shield having a thickness between 5 to 7 meters. However, in the case of the absorbed dose, the theory must use a restricted stopping power in order to get the best results

(use of an unrestricted stopping power results in a theoretical value that is 25% too high). The coherent production of muons, by itself, is adequate for good agreement at zero degrees.

(b) A constant "background" component is observed in the dose measurements, but it is not seen in the fluence measurements. The source is believed to be photons that originate in the dump and scatter over the top of the wall through relatively thin shielding. Because of the scattering angles involved, these photons most likely are low energy. Even though the secondary electrons produced by these photons register on the TLD, the voltage-discrimination of the scintillation counters and the visual discrimination of these tracks in the emulsion prevent them from being counted in the muon fluence measurements (Nelson 1973).

(c) The theory gradually disagrees with the measurements as the detector angle increases, the measurements being larger. At the largest detector angle (about 150 milliradians), the measurements are, in fact, 20 to 30 times higher than the coherent production theory predicts. By integrating under the respective curves, the total experimental muon yield (i.e., muons/Coulomb) is found to be 32% higher than the yield predicted by the coherent theory.

(d) Sources located other than at the main target-dump are ruled-out because of the symmetry in the vertical and horizontal data, and because of the angular distribution of tracks in the emulsion. The angular distribution measurements taken in the zero degree direction result in a narrow histogram that is symmetric (within statistics) about zero degrees. The angular distribution at 7.7 degrees consists of two peaks superimposed on an isotropic background. The larger of the two peaks is quite narrow and is centered at about 8 degrees, suggesting a direct component of muons from the source. The second, much

smaller, peak is centered at approximately 22 degrees and is relatively broader and might be explained by multiple scattering.

(e) A beryllium target, inserted in the beam just ahead of the dump, is observed to increase the muon fluence at the wide angles, but doesn't change the value at zero degrees. The increase is substantial; a factor of four in the case of an 18 GeV electron beam, and a factor of two for the 14 GeV case. The possibility of pions (or kaons) causing this effect is consistent with the larger peak in the angular distribution data at wide angles. Calculations, however, do not support the pion (kaon) decay hypothesis.

(f) The theoretical muon fluence (absorbed dose) that is presented for comparison with the measurements contains a number of approximations. Particularly, the inelastic nucleon scattering contribution, as well as certain elastic nucleon scattering terms are excluded. It is estimated, however, that the largest increase will amount to no more than 100% of the coherent contribution in the wide angle region, and therefore can not account for the observed discrepancy factor of 20 to 30.

(g) Other possible explanations, such as, shower divergence, electron/hadron contamination, or the effect of the void (found in the main shielding wall after the exposures had been made), fail to explain the large number of muons at the sides. Single scattering is suggested as a possible explanation. But only because the available theoretical results (Alsmiller 1969), that have been published to check this effect under similar conditions, do not extend far enough out in detector position.

From a health physics point of view, this study has been quite successful. The muon dose rate in the zero degree direction can be theoretically predicted with an uncertainty of ±10%. The dose rate at positions off the beam axis can,

with the help of the experimental observations, be estimated to about ±25%. The reason for the large fluence of muons at the wide angles, however, remains unknown at this time. A yet undiscovered source of muon production, that dominates at large production angles, could provide an explanation for our observations.

ACKNOWLEDGMENTS

The authors wish to acknowledge the support and help from the Health Physics and Operation crews at SLAC. The mechanical structures and devices were constructed under the supervision of J. Zabdyr and A. Baumgarten, and we appreciate their help. We are also grateful for many discussions with Drs. R. C. McCall, H. DeStaebler, Jr., R. Mozley, B. Richter, A. Leonard, and W. Swanson. A particular thanks goes to Dr. J. Lord (University of Washington) for developing the emulsions and for many useful suggestions. The accelerator time, obtained for us by Dr. W. K. H. Panofsky, is extremely appreciated.

REFERENCES

R. G. Alsmiller, Jr., M. Leimdorfer, and J. Barish, High-energy muon transport and the muon backstop for a 200-GeV proton accelerator, Oak Ridge National Laboratory Report Number ORNL-4322, Oak Ridge, Tennessee (1968).

R. G. Alsmiller, Jr., High-energy (< 18 GeV) muon transport calculations and comparison with experiment, Nucl. Instr. Meth. 71 (1969),121.

R. G. Alsmiller, Jr. and J. Barish, High-energy muon transport and the muon backstop for a multi-GeV proton accelerator, Oak Ridge National Laboratory Report Number ORNL-4386, Oak Ridge, Tennessee (1969).

R. G. Alsmiller, Jr., F. S. Alsmiller, J. Barish, and Y. Shima, Muon transport and the shielding of high-energy ($\leq$ 500 GeV) proton accelerators, Proceedings of the International Congress on Protection Against Accelerator and Space Radiation, CERN-71-16, Volume 2, Geneva, Switzerland (1971).

M. J. Berger and S. M. Seltzer, Tables of energy losses and ranges of electrons and positrons, National Aeronautics and Space Administration Report Number NASA-SP-3012 (1964).

M. J. Berger and S. M. Seltzer, Additional stopping power and range tables for protons, mesons, and electrons, National Aeronautics and Space Administration Report Number NASA-SP-3036 (1966).

O. I. Dovzhenko and A. A. Pomanskii, Radiation units and critical energies for various substances, Sov. Phys. JETP 18 (1964),187.

L. Eyges, Multiple scattering with energy loss, Phys. Rev. 74 (1948),1534.

R. Gay and G. Svensson, A discussion of an experimental evaluation of the use of the fission fragment track registration method for particle fluence measurements, Stanford Linear Accelerator Center Report Number SLAC-TN-70-33, Stanford University, Stanford, California (1970).

J. L. Harris, S. K. Howry, E. J. Seppi, and H. A. Weidner, Beam Switchyard design and operation, The Stanford Two-Mile Accelerator, Chapter 17, R. B. Neal (Ed.), (New York: W. A. Benjamin) (1968).

K. J. Kim and Y. S. Tsai, An improved Weizsaker-Williams method and photoproduction of lepton pairs, Phys. Letters 40B (1972a),662.

K. J. Kim and Y. S. Tsai, Improved Weizsacker-Williams method and its application to lepton and W-boson pair production, Stanford Linear Accelerator Center Report Number SLAC-PUB-1106 (Rev.), Stanford University, Stanford, California (1973).

R. S. Larsen, Design of beam position and charge monitoring circuits for the Stanford two-mile accelerator, Stanford Linear Accelerator Center Report Number SLAC-63, Stanford University, Stanford, California (1966).

R. S. Larsen and D. Horelick, A precision toroidal charge monitor for SLAC, Stanford Linear Accelerator Report Number SLAC-PUB-398, Stanford University, Stanford, California (1968).

G. Moliere, Theorie der streuung schneller geladener teilchen I: einzelstreuung am abgeschirmten Coulombfeld, Z. Naturf. 2a (1947), 133; Z. Naturf. 3a (1948), 78.

W. R. Nelson, The shielding of muons around high-energy electron accelerators: theory and measurement, Nucl. Instr. Meth. 66 (1968),293.

W. R. Nelson, The shielding of muons around high energy electron accelerators: theory and measurement, Ph. D. Thesis, Graduate Division Special Program, Stanford University, Stanford, California (1973).

B. Rossi, High-Energy Particles (Englewood Cliffs, New Jersey: Prentice Hall (1952)).

SLAC Users Handbook, Stanford Linear Accelerator Center, Stanford University, Stanford, California (1971).

G. K. Svensson, R. C. McCall, and G. Babcock, An improved TLD reader, Stanford Linear Accelerator Center Report Number SLAC-PUB-731, Stanford University, Stanford, California (1970).

Y. Tsai and V. Whitis, Thick-target bremsstrahlung and target considerations for secondary-particle production by electrons, Phys. Rev. 149 (1966),1248.

Y. S. Tsai, Estimates of secondary-beam yields at SLAC, SLAC Users Handbook, C. 3-1, Stanford Linear Accelerator Center, Stanford, California (1971).

C. D. Zerby and H. S. Moran, Studies of the longitudinal development of high-energy electron-photon cascade showers in copper, Oak Ridge National Laboratory Report Number ORNL-3329, Oak Ridge, Tennessee (1962a).

C. D. Zerby and H. S. Moran, A Monte Carlo calculation of the three-dimensional development of high-energy electron-photon cascade showers, Oak Ridge National Laboratory Report Number ORNL-TM-422, Oak Ridge, Tennessee (1962b).

C. D. Zerby and H. S. Moran, Studies of the longitudinal development of electron-photon cascade showers, J. Appl. Phy. 34 (1963),2445.

Table 1

GAP	SOURCE-TO-DETECTOR DISTANCE, R(cm)	SHIELD THICKNESS, d(cm) NO VOID	VOID
A	555.19	509.91	480.06
B	629.34	565.79	535.94
C	703.00	622.68	592.84
D	775.87	679.58	649.73

Table 2

THE EFFECT OF BERYLLIUM TARGET ON MUON YIELDS

	SC1: Theta = 0 mradians		SC2: Theta = 154 mradians	
Energy	Be Out	Be In	Be Out	Be In
18 GeV	2.18×10^{10}	2.07×10^{10}	1.10×10^{6}	4.60×10^{6}
14 GeV	6.67×10^{9}	6.67×10^{9}	0.97×10^{6}	1.90×10^{6}

Target length = 1.0 radiation length

Units are muons/sq.cm/Coulomb

Table 3

MUON FLUENCE FROM PI AND K DECAY (GAP A)

Theta (mradians)	Pi-decay fluence (muons/sq.cm/Coul.)	K-decay fluence (muons/sq.cm/Coul.)
0	2.58×10^{7}	4.62×10^{6}
10	2.47×10^{7}	4.48×10^{6}
20	2.18×10^{7}	4.08×10^{6}
30	1.77×10^{7}	3.51×10^{6}
40	1.34×10^{7}	2.85×10^{6}
50	9.56×10^{6}	2.21×10^{6}
60	6.47×10^{6}	1.64×10^{6}
70	4.18×10^{6}	1.16×10^{6}
80	2.61×10^{6}	7.99×10^{5}
90	1.58×10^{6}	5.34×10^{5}
100	9.32×10^{5}	3.49×10^{5}
110	5.41×10^{5}	2.22×10^{5}
120	3.11×10^{5}	1.39×10^{5}
130	1.78×10^{5}	8.61×10^{4}
140	1.03×10^{5}	5.24×10^{4}
150	5.94×10^{4}	----

FIGURE CAPTIONS

1. Plan view of the experimental set-up.
2. Elevation view of the experimental set-up.
3. End view of the experimental set-up.
4. Photograph of the detector stand-array without the shielding around it.
5. Photograph of the detector stand-array with the iron shielding around it.
6. Photomicrograph showing three muon tracks in a nuclear emulsion plate.
7. Muon fluence versus angle for Gap A.
8. Muon fluence versus angle for Gap B.
9. Muon fluence versus angle for Gap C.
10. Muon fluence versus angle for Gap D.
11. Absorbed dose versus angle for Gap A.
12. Absorbed dose versus angle for Gap B.
13. Absorbed dose versus angle for Gap C.
14. Absorbed dose versus angle for Gap D.
15. Comparison of the measured absorbed dose (TLD) and the calculated absorbed dose (from nuclear emulsion and scintillation counter data) with theory as a function of angle.
16. Angular distribution of tracks in the forward direction (zero degrees).
17. Angular distribution of tracks at 7.7 degrees and comparison with calculation.
18. Comparison of the π/k muon decay fluence with the coherent pair production fluence and with measurement.

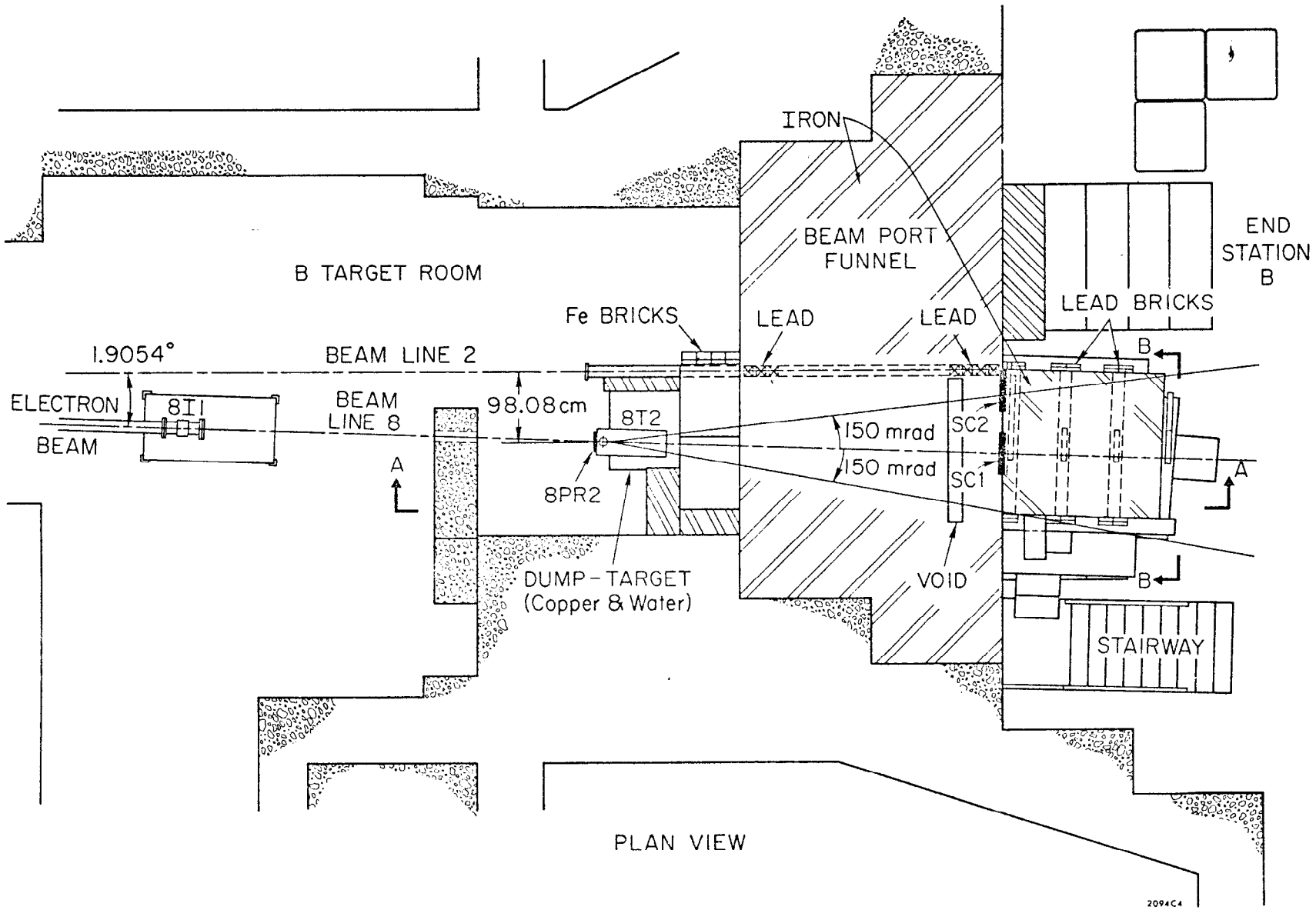
IRON
BEAM PORT
FUNNEL
END
STATION
B
B TARGET ROOM
LEAD BRICKS
Fe BRICKS
LEAD
LEAD
1.9054°
BEAM LINE 2
B
ELECTRON
BEAM
8I1
BEAM
LINE 8
98.08cm
8T2
150 mrad
150 mrad
SC2
SC1
A
A
8PR2
DUMP – TARGET
(Copper & Water)
VOID
B
STAIRWAY
PLAN VIEW
2094C4

Fig. 1

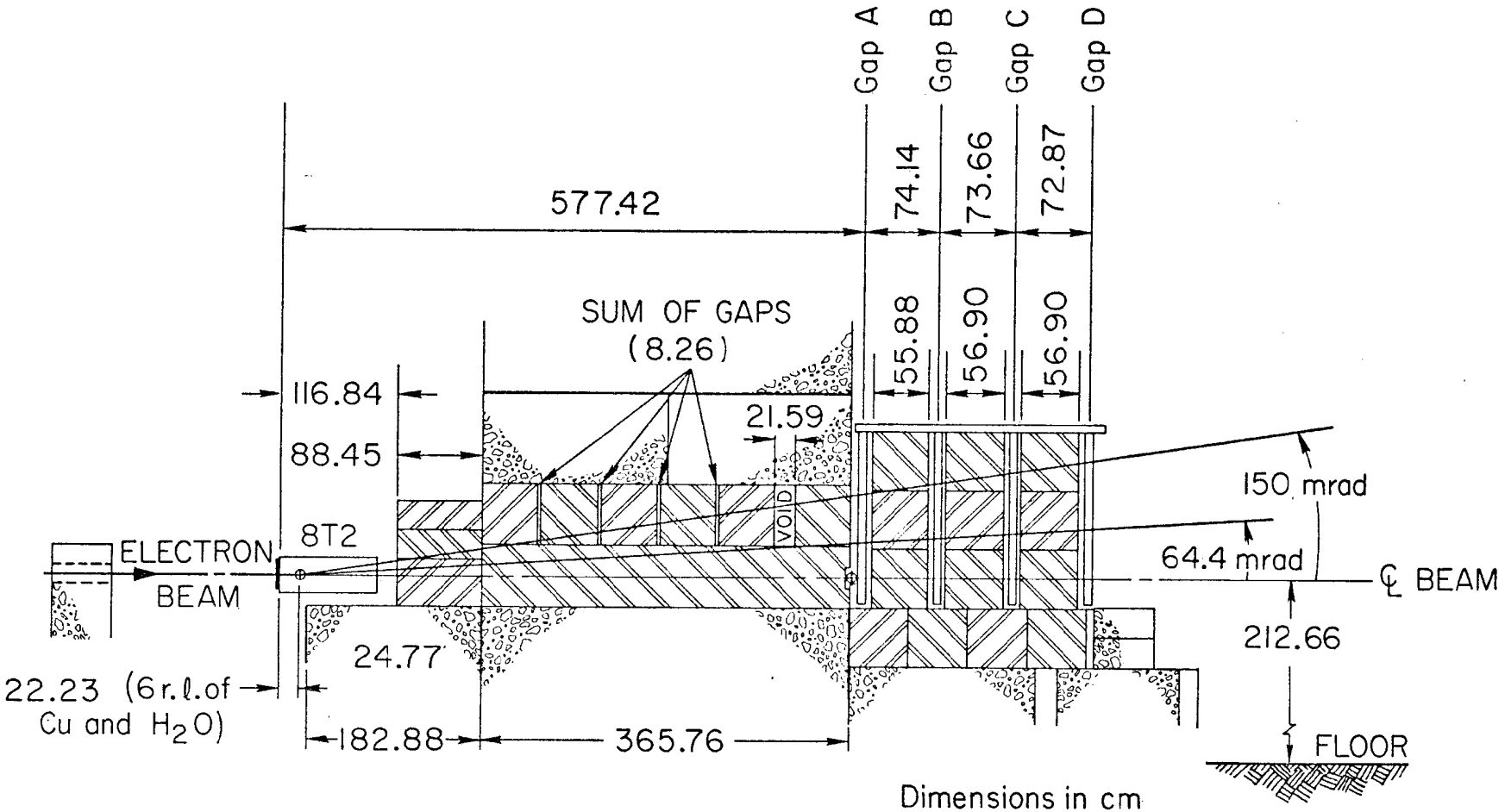
Gap A
Gap B
Gap C
Gap D
577.42
74.14
73.66
72.87
SUM OF GAPS
(8.26)
55.88
56.90
56.90
116.84
88.45
21.59
VOID
150 mrad
64.4 mrad
ELECTRON
BEAM
8T2
℄ BEAM
212.66
24.77
22.23 (6 r.l. of
Cu and H_2O)
182.88
365.76
FLOOR
Dimensions in cm
Section A-A
2094C2

Fig. 2

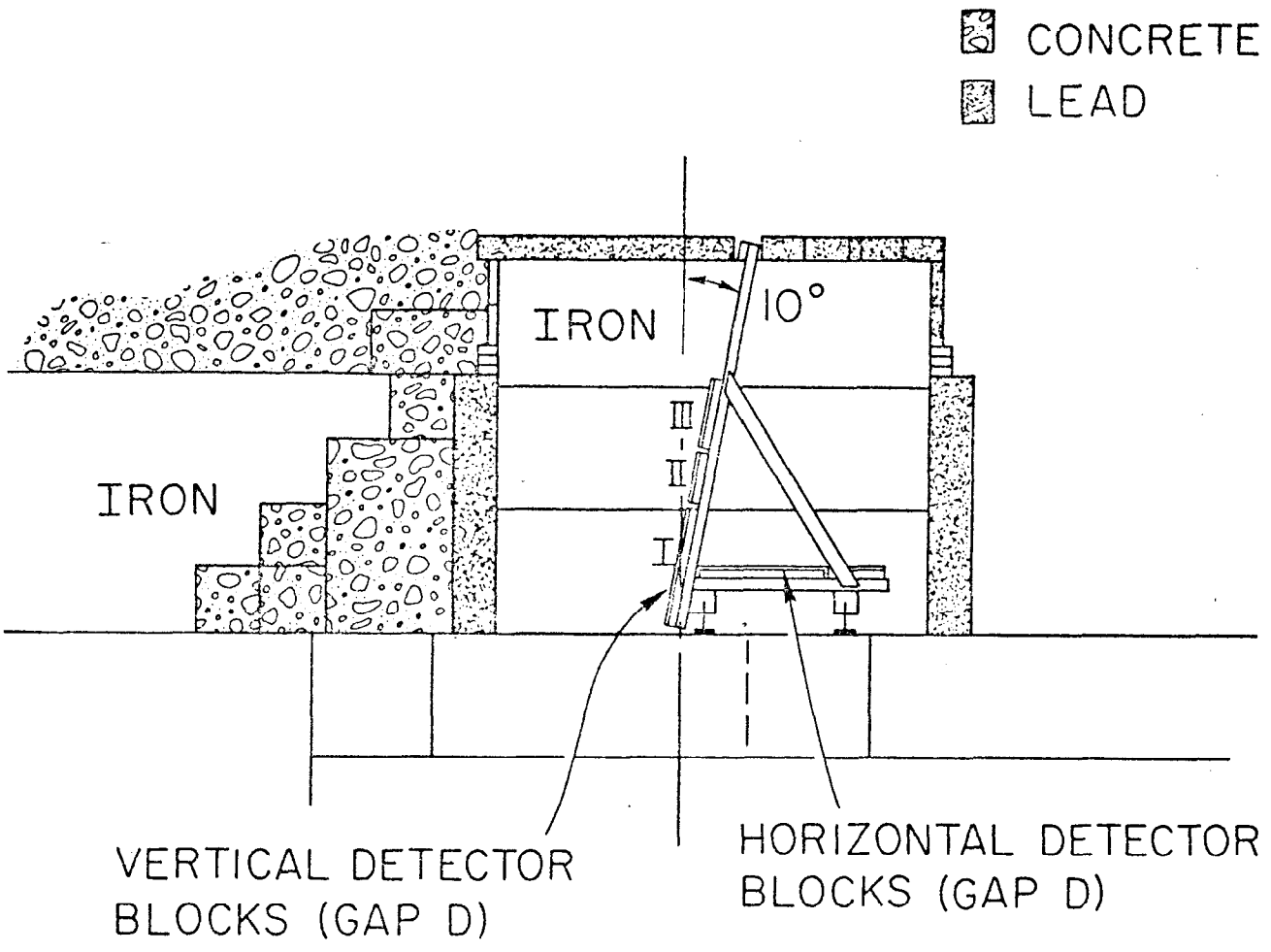

Section B-B

2093A3

Fig. 3

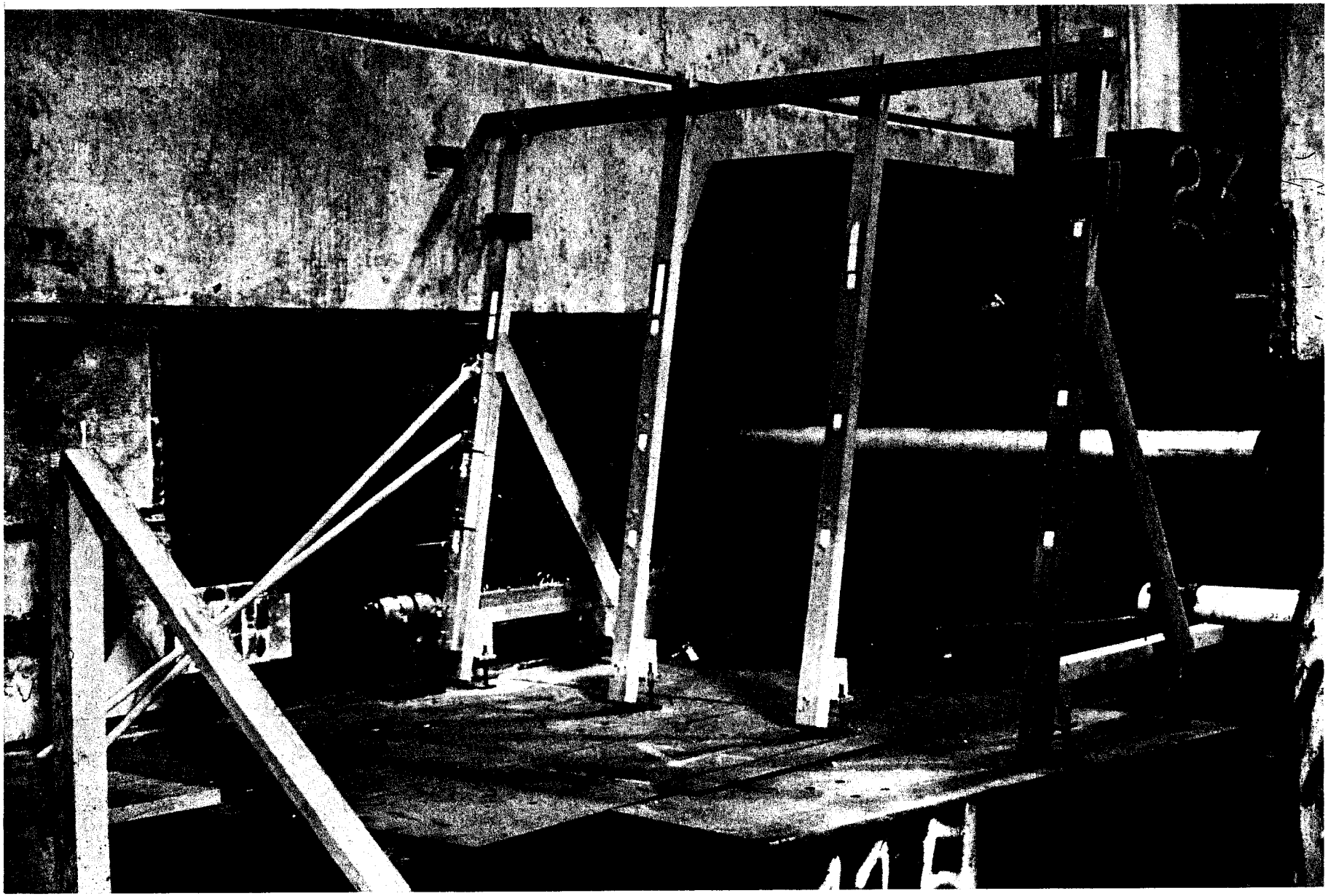

Fig. 4

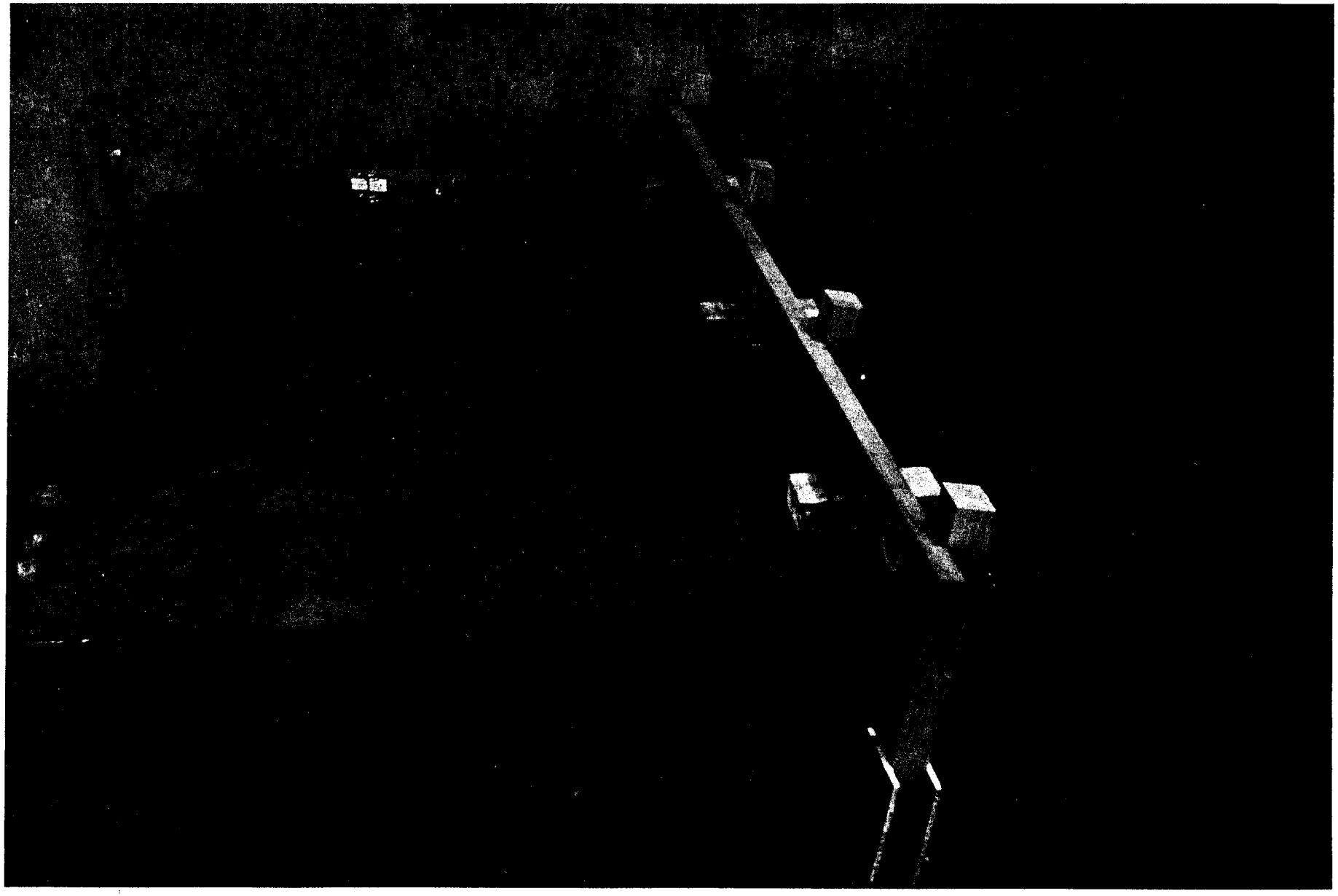

Fig. 5

Fig. 6

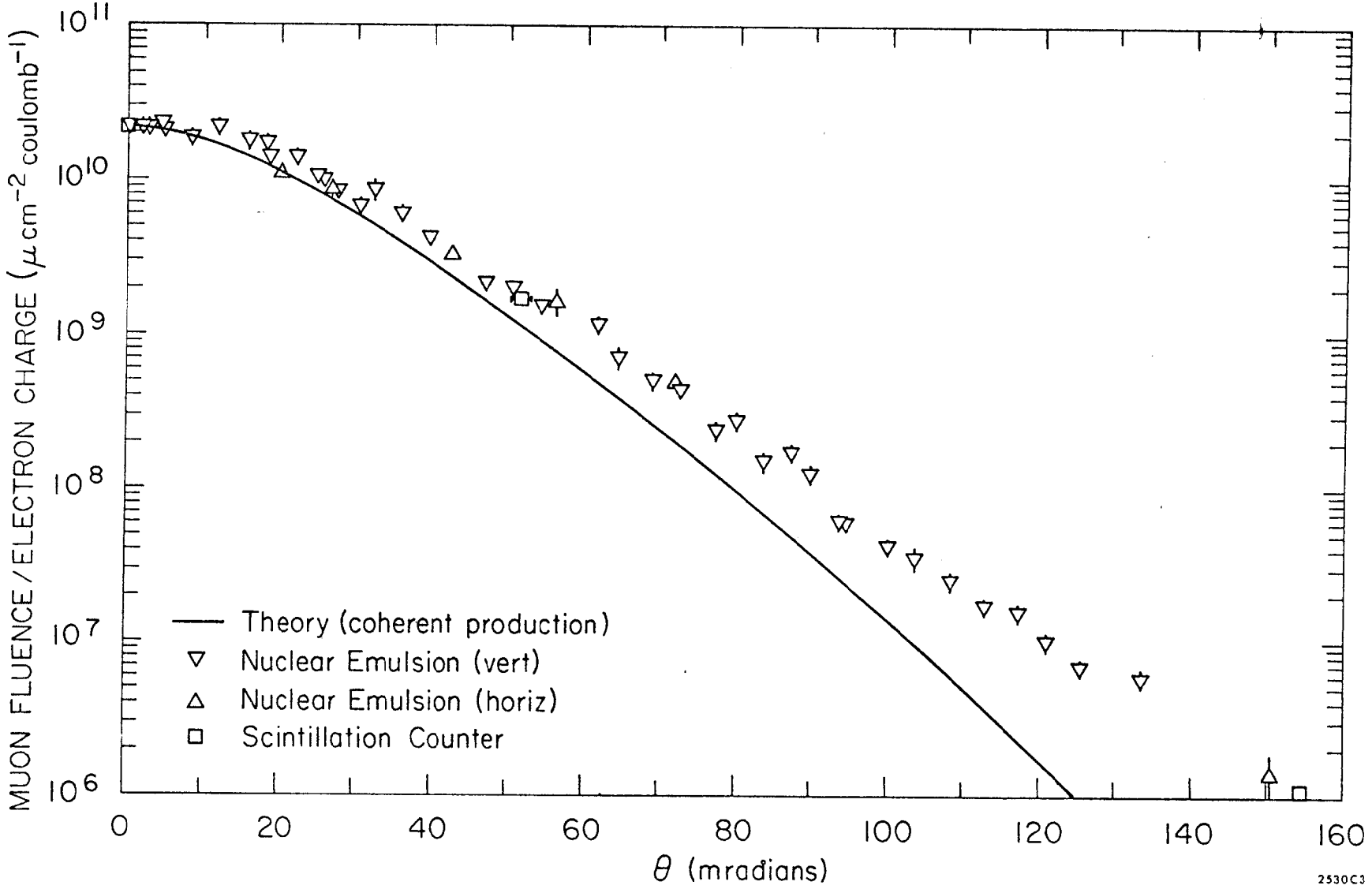
MUON FLUENCE / ELECTRON CHARGE (μ cm^{-2} coulomb^{-1})
10^{11}
10^{10}
10^{9}
10^{8}
10^{7}
10^{6}
0
20
40
60
80
100
120
140
160
θ (mradians)
Theory (coherent production)
Nuclear Emulsion (vert)
Nuclear Emulsion (horiz)
Scintillation Counter
2530C3

Fig. 7

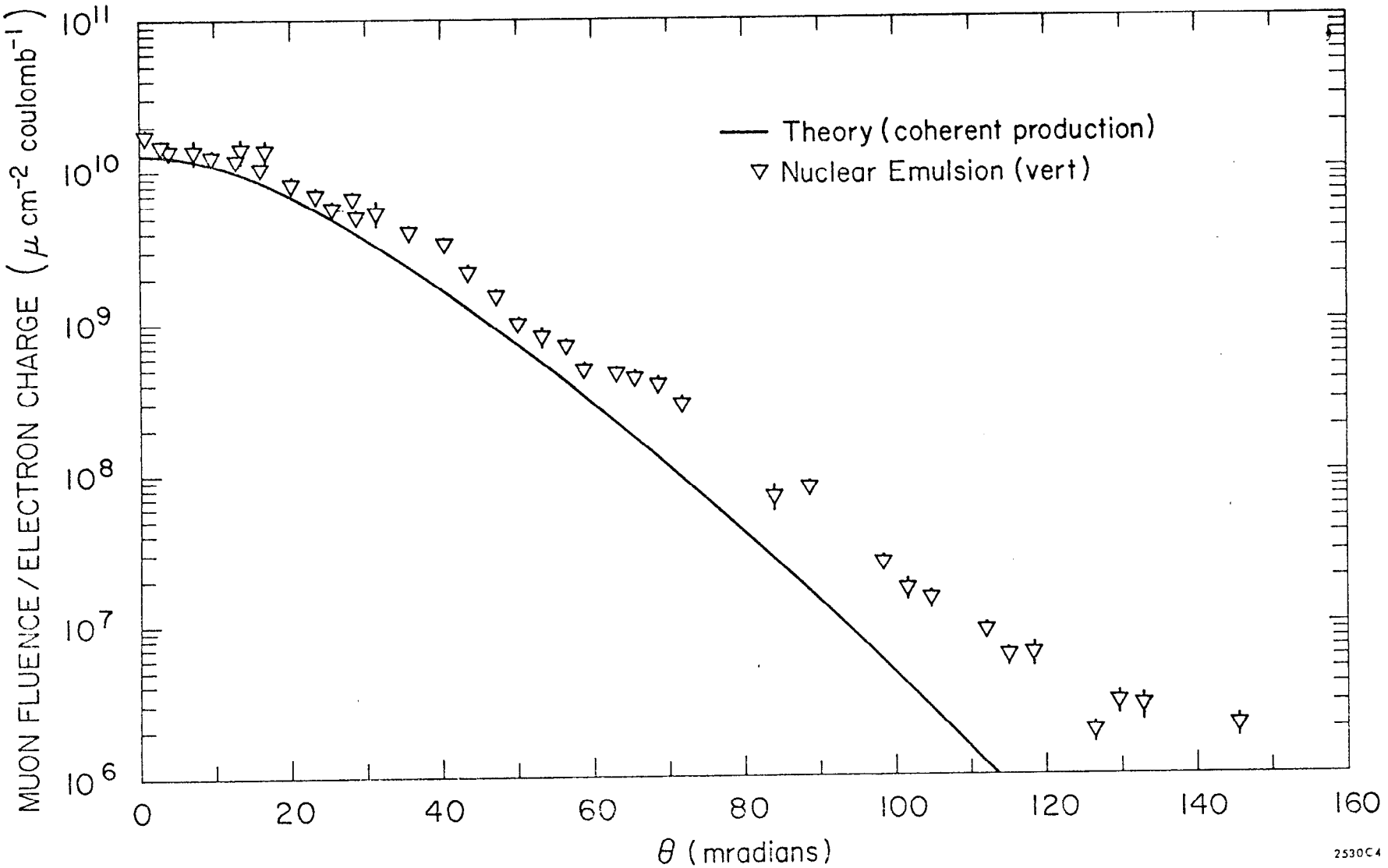
MUON FLUENCE / ELECTRON CHARGE (μ cm^{-2} coulomb^{-1})
10^{11}
10^{10}
10^{9}
10^{8}
10^{7}
10^{6}
0
20
40
60
80
100
120
140
160
θ (mradians)
Theory (coherent production)
Nuclear Emulsion (vert)
2530C4

Fig. 8

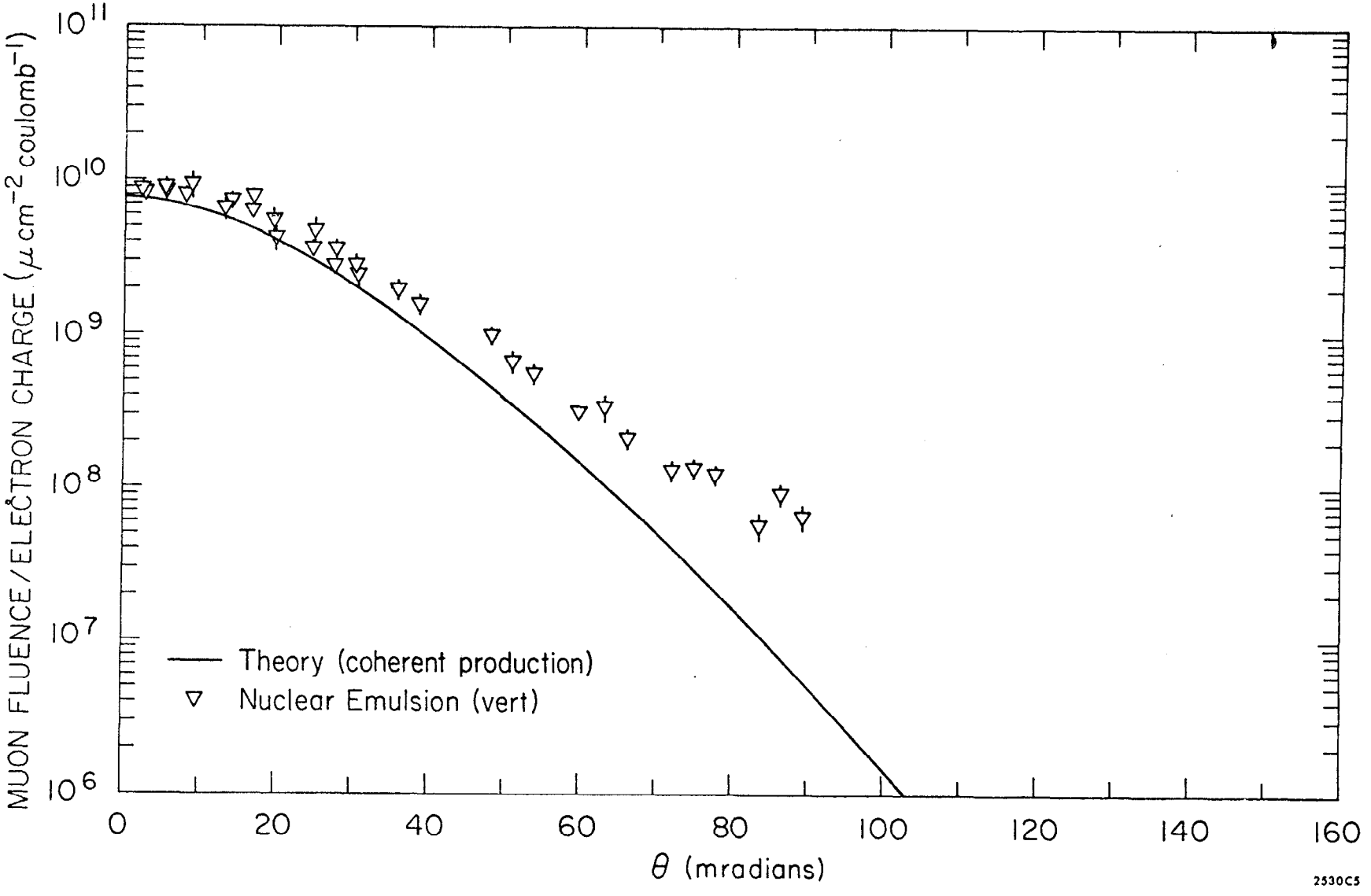
MUON FLUENCE / ELECTRON CHARGE (μ cm^{-2} coulomb^{-1})
10^{11}
10^{10}
10^{9}
10^{8}
10^{7}
10^{6}
0
20
40
60
80
100
120
140
160
θ (mradians)
Theory (coherent production)
Nuclear Emulsion (vert)
2530C5

Fig. 9

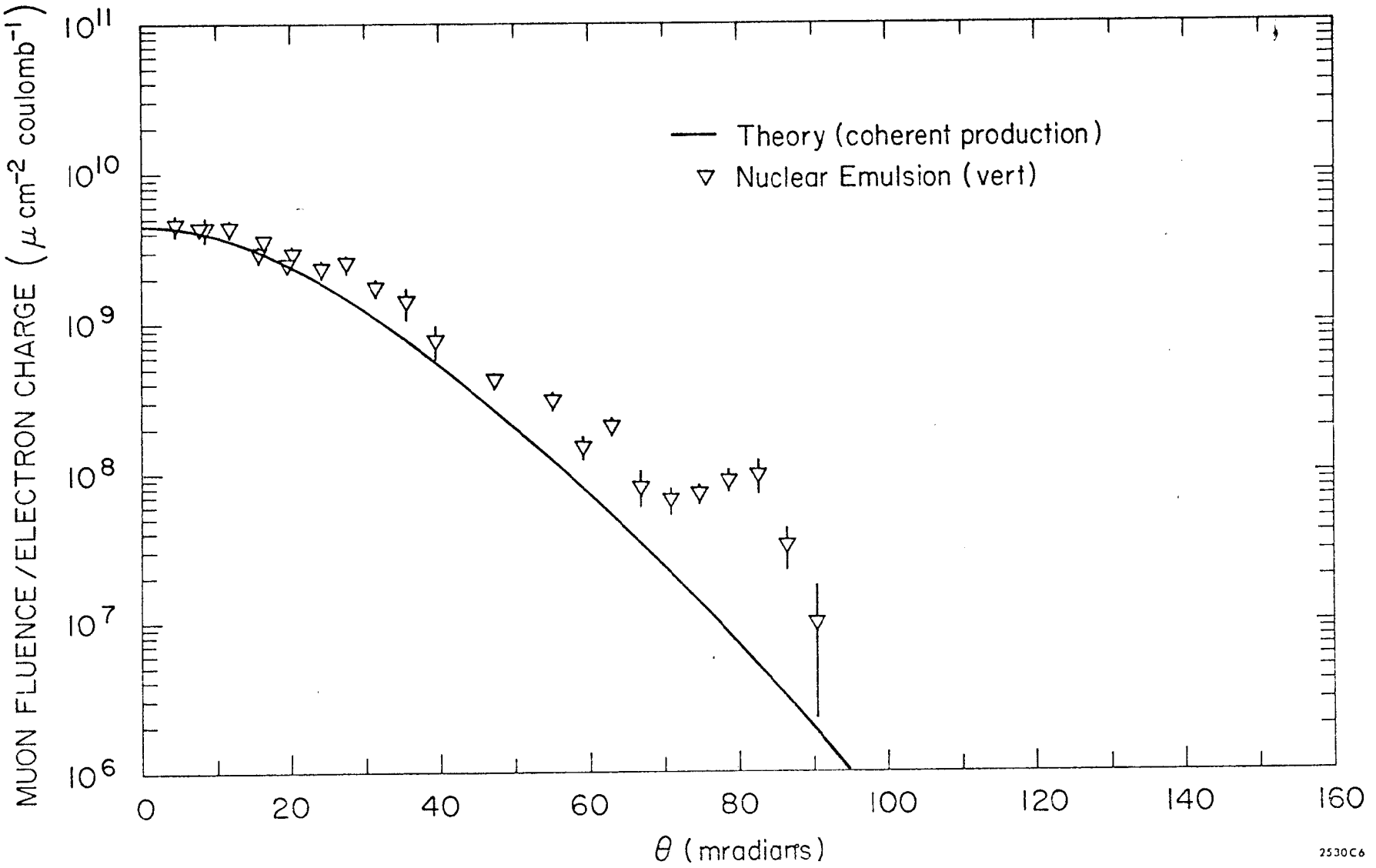
MUON FLUENCE/ELECTRON CHARGE (μ cm^{-2} coulomb^{-1})
10^{11}
10^{10}
10^{9}
10^{8}
10^{7}
10^{6}
0
20
40
60
80
100
120
140
160
θ (mradians)
Theory (coherent production)
Nuclear Emulsion (vert)
2530C6

Fig. 10

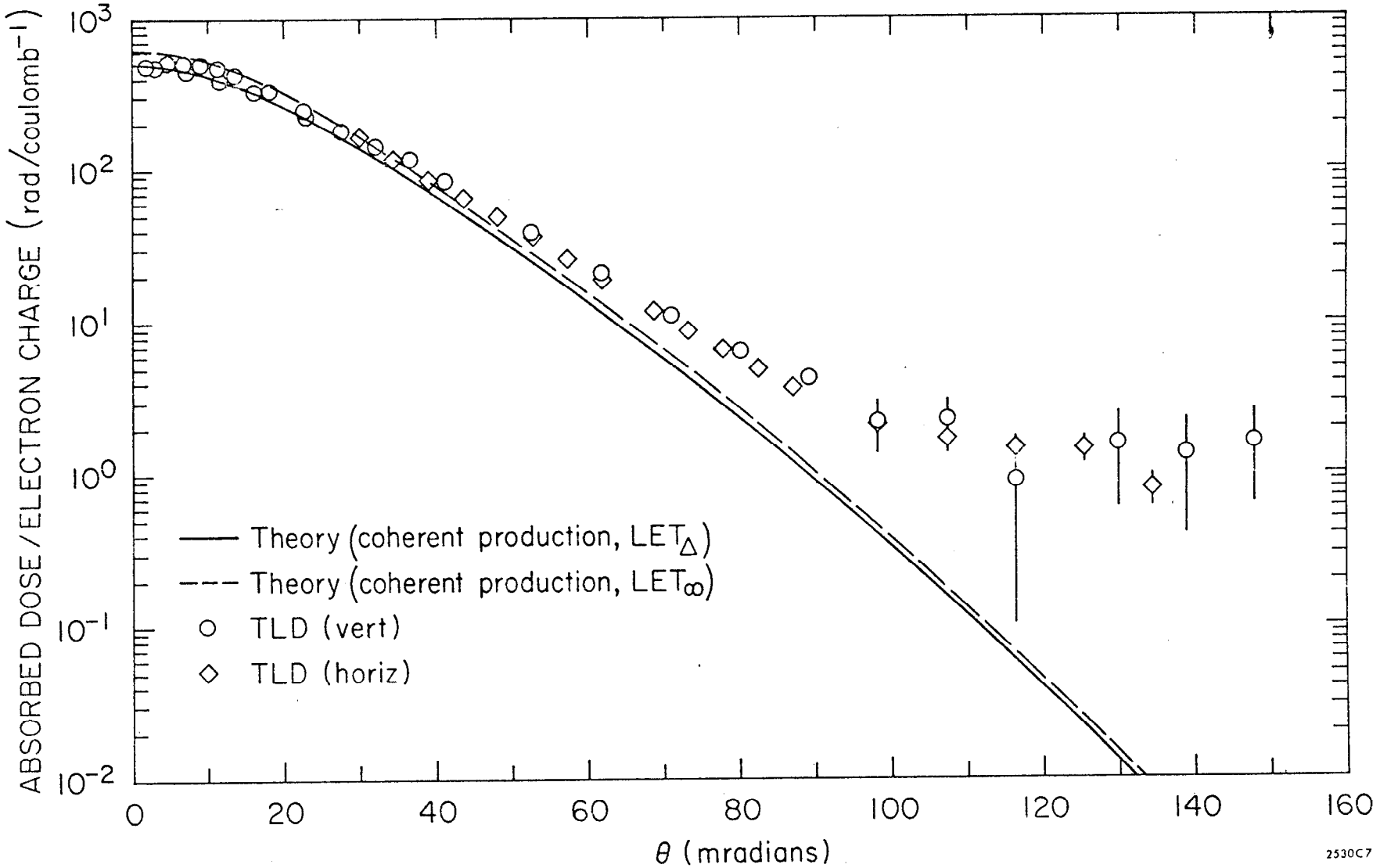
ABSORBED DOSE / ELECTRON CHARGE (rad/coulomb⁻¹)
10³
10²
10¹
10⁰
10⁻¹
10⁻²
0
20
40
60
80
100
120
140
160
θ (mradians)
Theory (coherent production, LET_Δ)
Theory (coherent production, LET_∞)
TLD (vert)
TLD (horiz)
2530C7

Fig. 11

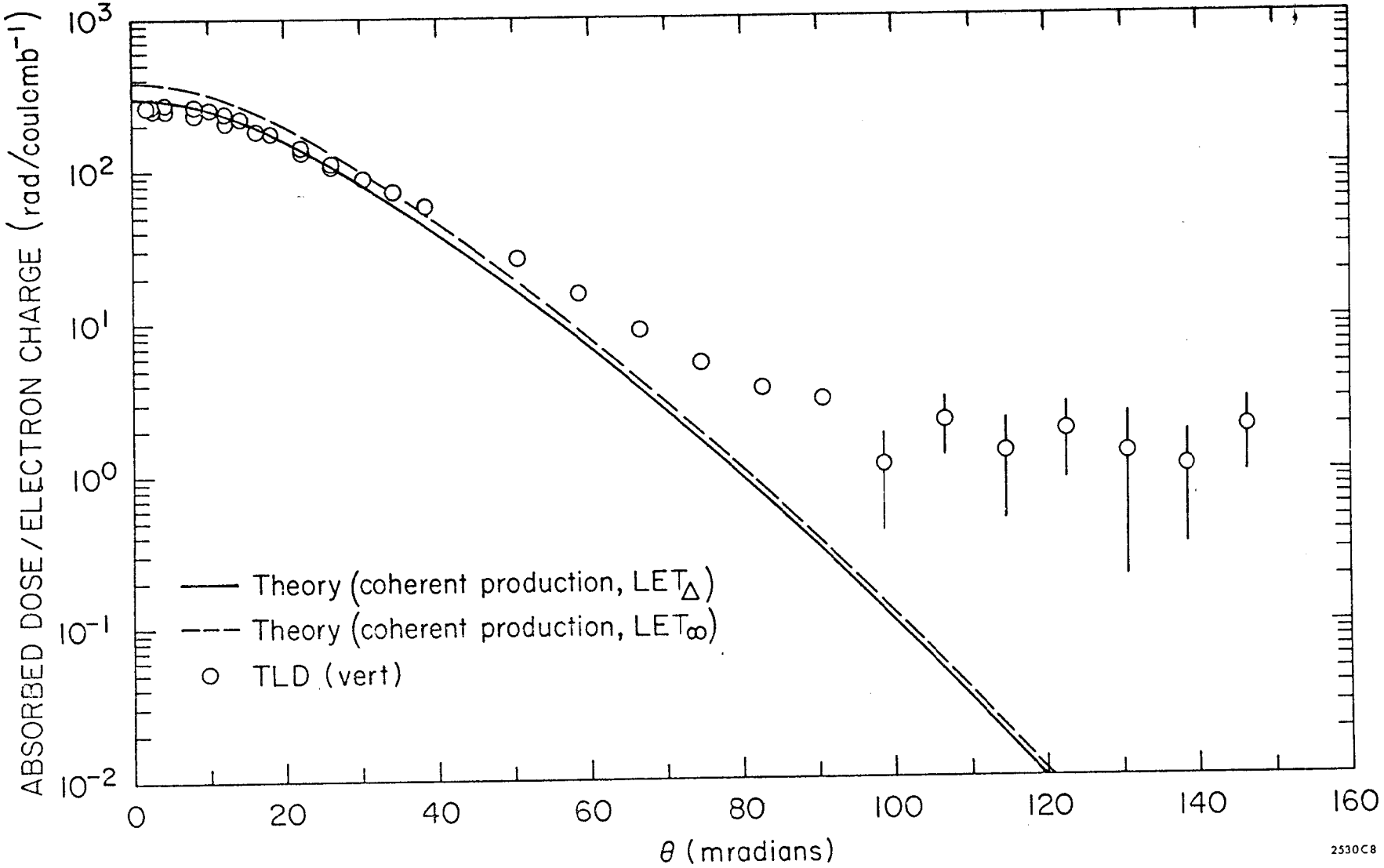
ABSORBED DOSE / ELECTRON CHARGE (rad/coulomb⁻¹)
10³
10²
10¹
10⁰
10⁻¹
10⁻²
0
20
40
60
80
100
120
140
160
θ (mradians)
Theory (coherent production, LET_Δ)
Theory (coherent production, LET_∞)
TLD (vert)
2530C8

Fig. 12

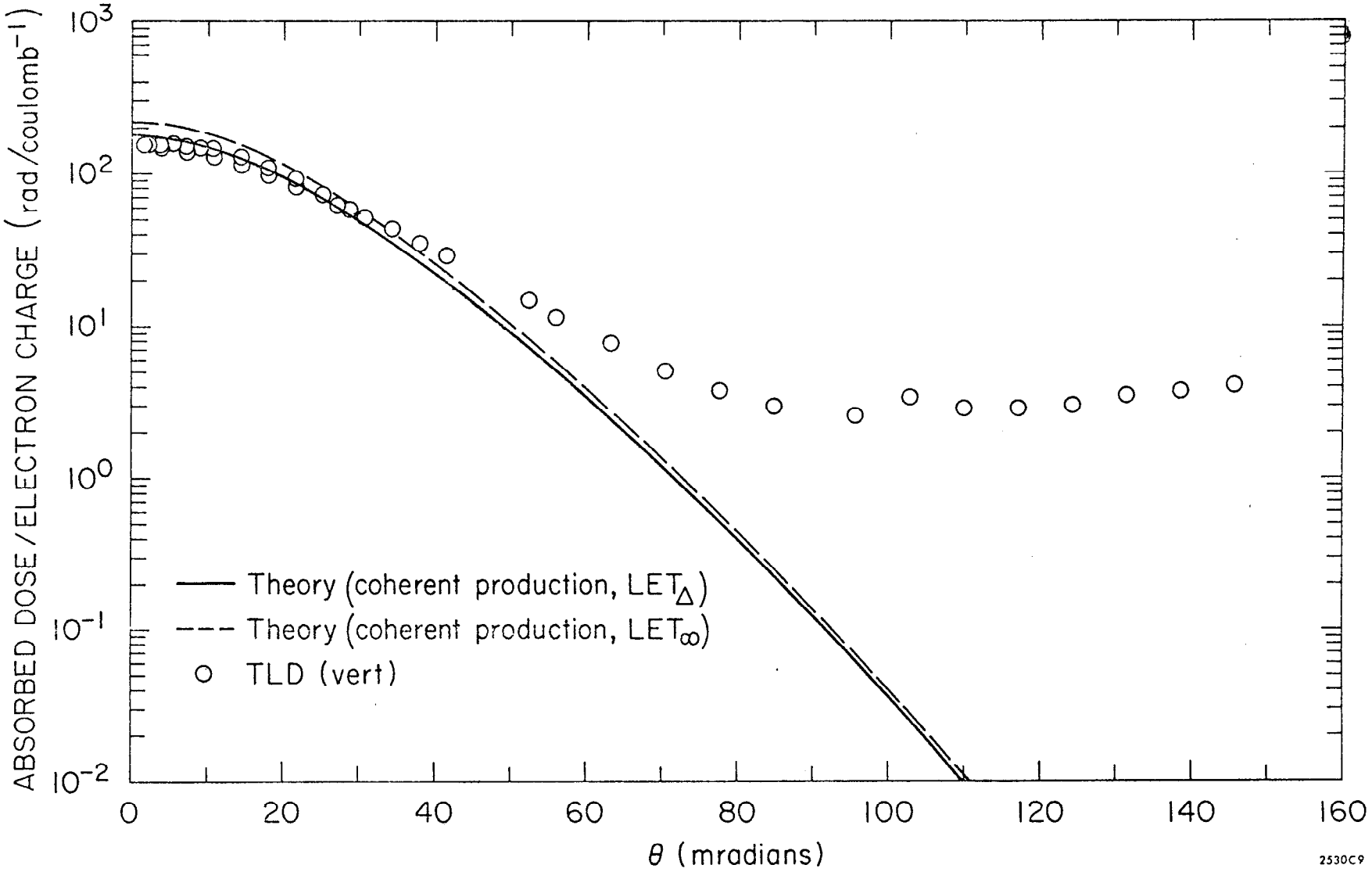
ABSORBED DOSE/ELECTRON CHARGE (rad/coulomb^{-1})
10^3
10^2
10^1
10^0
10^{-1}
10^{-2}
0
20
40
60
80
100
120
140
160
θ (mradians)
Theory (coherent production, LET$_\Delta$)
Theory (coherent production, LET$_\infty$)
TLD (vert)
2530C9

Fig. 13

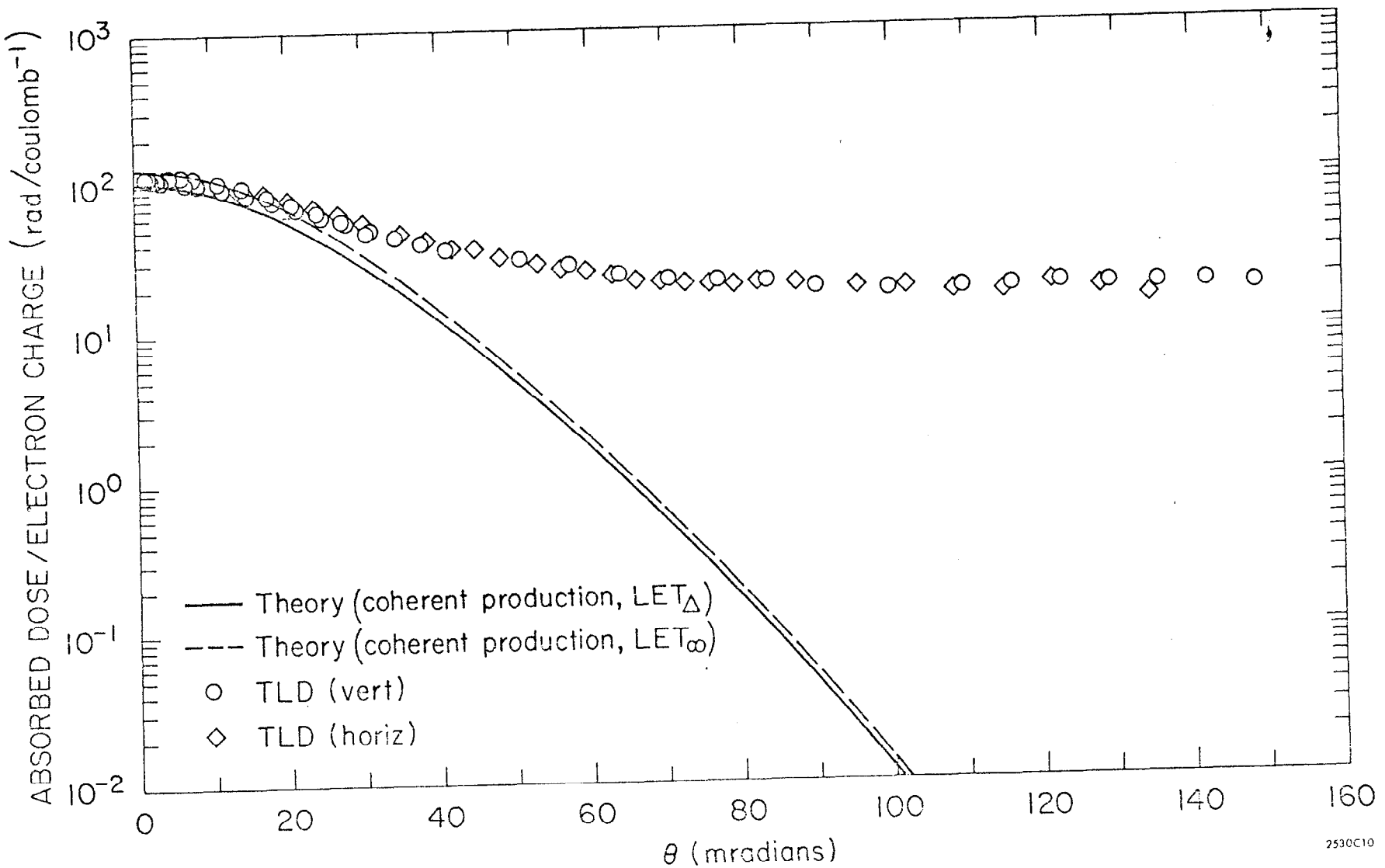
ABSORBED DOSE / ELECTRON CHARGE (rad/coulomb^{-1})
10^3
10^2
10^1
10^0
10^{-1}
10^{-2}
0
20
40
60
80
100
120
140
160
θ (mradians)
Theory (coherent production, LET$_\Delta$)
Theory (coherent production, LET$_\infty$)
TLD (vert)
TLD (horiz)
2530C10

Fig. 14

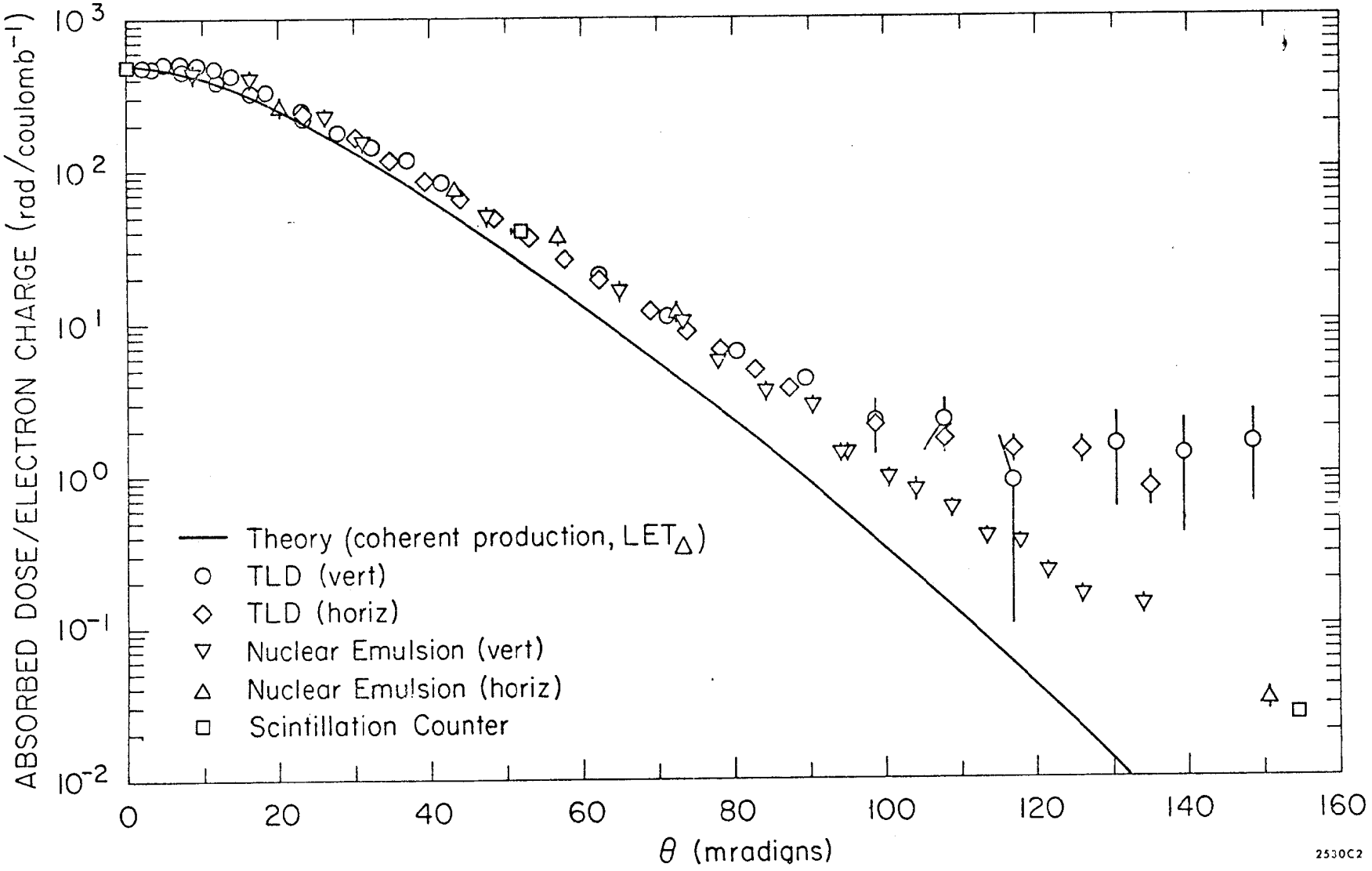
ABSORBED DOSE/ELECTRON CHARGE (rad/coulomb^{-1})
10^3
10^2
10^1
10^0
10^{-1}
10^{-2}
0
20
40
60
80
100
120
140
160
θ (mradians)
Theory (coherent production, LET$_\Delta$)
TLD (vert)
TLD (horiz)
Nuclear Emulsion (vert)
Nuclear Emulsion (horiz)
Scintillation Counter
2530C2

Fig. 15

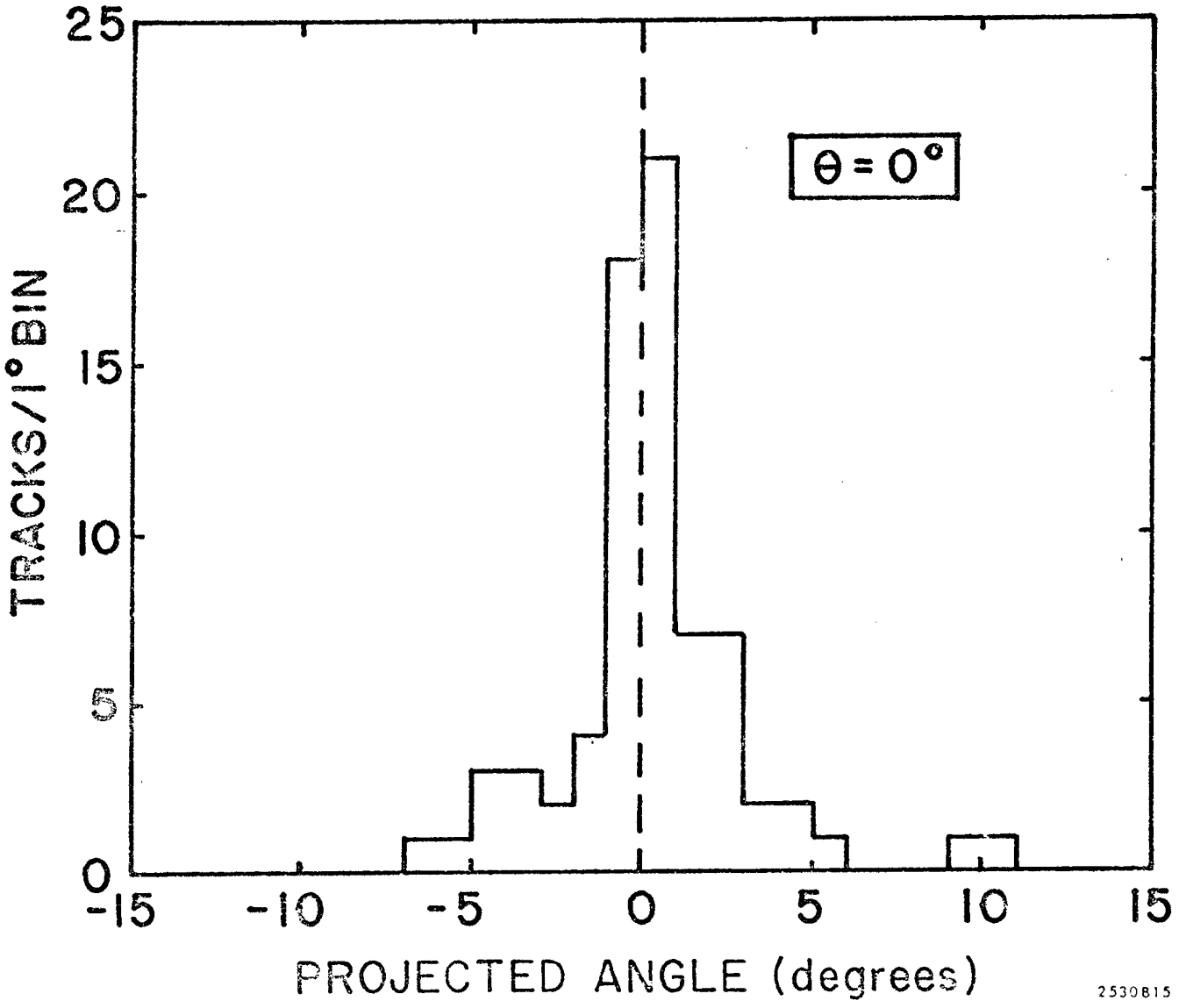
θ = 0°
TRACKS/1° BIN
PROJECTED ANGLE (degrees)
25
20
15
10
5
0
-15
-10
-5
0
5
10
15
2530815

Fig. 16

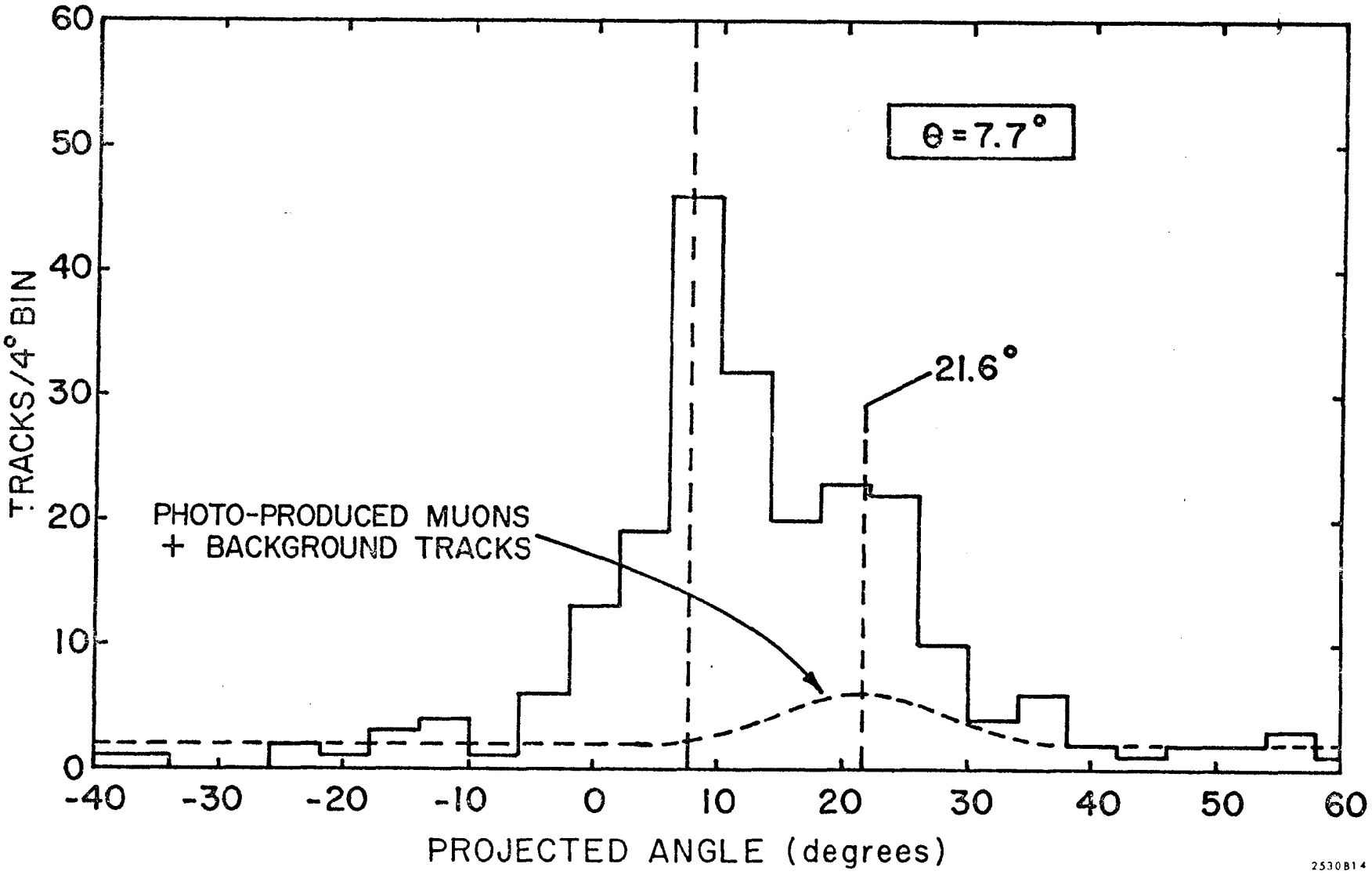
θ = 7.7°
21.6°
PHOTO-PRODUCED MUONS
+ BACKGROUND TRACKS
TRACKS/4° BIN
PROJECTED ANGLE (degrees)
0
10
20
30
40
50
60
-40
-30
-20
-10
0
10
20
30
40
50
60
2530B14

Fig. 17

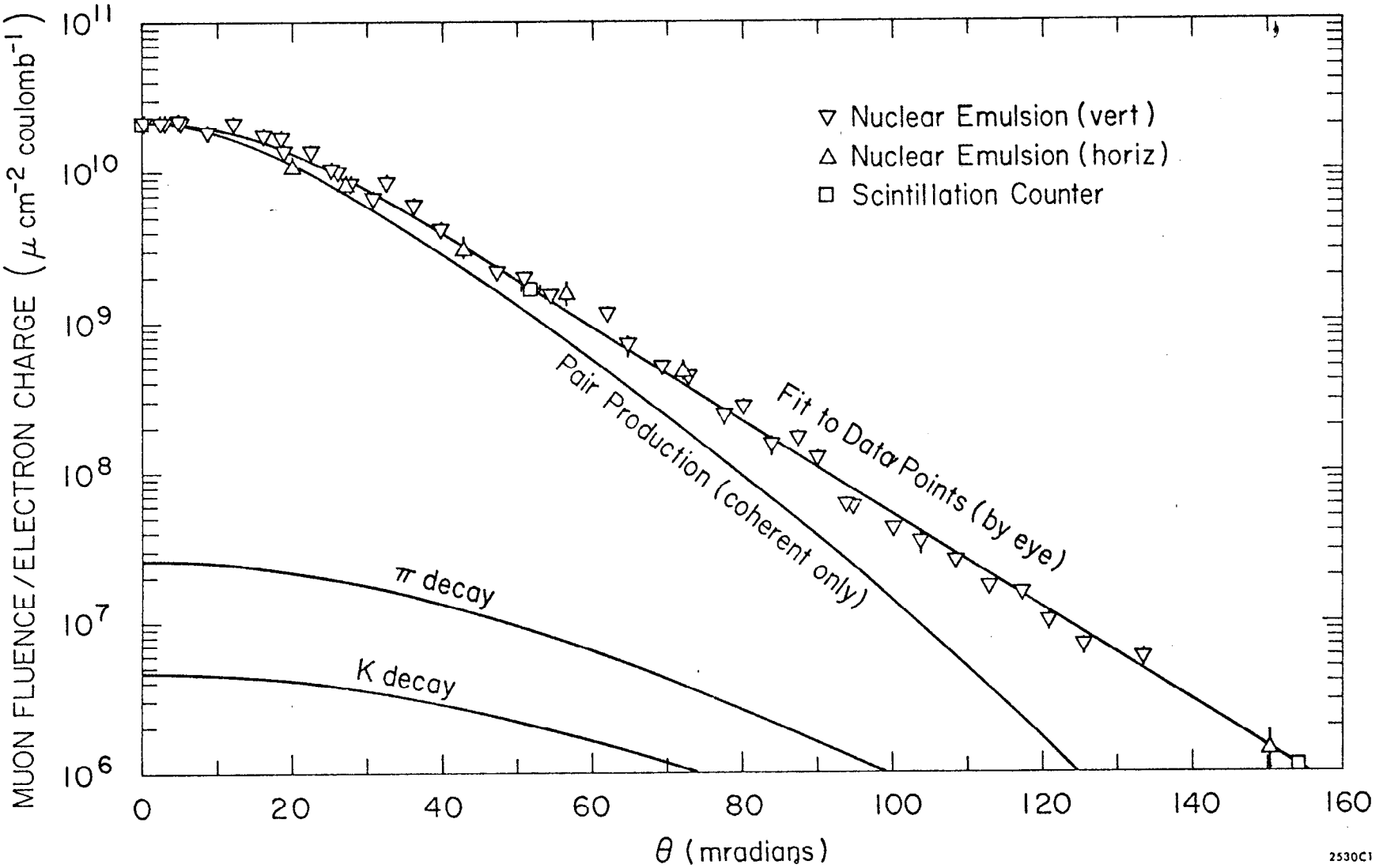
MUON FLUENCE/ELECTRON CHARGE (μ cm^{-2} coulomb^{-1})
10^{11}
10^{10}
10^{9}
10^{8}
10^{7}
10^{6}
0
20
40
60
80
100
120
140
160
θ (mradians)
▽ Nuclear Emulsion (vert)
△ Nuclear Emulsion (horiz)
□ Scintillation Counter
Fit to Data Points (by eye)
Pair Production (coherent only)
π decay
K decay
2530C1

Fig. 18